# Design, Modelling, and Test of an Electromagnetic Speed Bump Energy Harvester

Prakhar Todaria

Thesis submitted to the faculty of the Virginia Polytechnic Institute and State University in partial fulfillment of the requirements for the degree of

Master of Science In
Mechanical Engineering

Lei Zuo, Chair

Saied Taheri

Linbing Wang

03/28/2016

Blacksburg, VA

Keywords: speed bump, energy harvester, modelling, design, vehicle dynamics

**Design, Modelling, and Test of an Electromagnetic Speed Bump Energy Harvester**

Prakhar Todaria

ABSTRACT

Speed bump energy harvester, which aims to harvest energy from the passing by vehicles by absorbing their kinetic and potential energy, is designed, fabricated, simulated, and tested in this research. The proposed design is analyzed with a theoretical modelling which has then been validated with a ground test. Result reveals that the prototype has been able to produce up to 600 watts of peak power and around 150 watts of RMS power which is significant number. Further analysis has been done which theoretically suggests that the numbers could be increased up to 1 KW by optimizing the speed bump design and varying the system parameters such as electrical damping, mechanical damping, velocity and weight of the vehicles. Overall, system is able to increase the overall energy density by using Mechanical Motion Rectification (MMR) technology which would allow the increase in the power generation almost by double. Furthermore, different vehicle models have been used to analyze the effectiveness and accuracy of the harvester and also, the effect of harvester on the dynamics of the vehicle has been studied and analyzed in detail.

**Design, Modelling, and Test of an Electromagnetic Speed Bump Energy Harvester**

Prakhar Todaria

General Audience Abstract

Speed bump energy harvester is a novel technique of harvesting energy from the passing vehicles on the streets and the road. This research is a study about the speed bump harvester, the amount of electricity it is capable of harvesting, its effects on the vehicle and ways to improve the energy generating capacity. In order to do this, a prototype was developed, tested, modelled and simulated which gives us a scientific insight of the entire concept. This system is capable of producing significant amount of energy which has been validated by a ground test.

The electricity thus generated by the system could be used to power on street electrical and electronic devices which can make the transportation more independent and versatile in nature.

# Acknowledgement

First and foremost, I would like to extend my sincerest gratitude to my graduate advisor, Prof. Lei Zuo, whose dedication towards the research has been an inspiration for me, whose unwavering academic support, collegiality, and mentorship throughout my entire graduate life, has helped me achieve my degree. I also can't be more thankful to him for spending countless hours proofreading my thesis and giving me suggestions on improving my writing.

I would also like to express my deep sense of gratitude to Prof. Said Taheri and Prof. Libing Wang, who have served as my graduate thesis committee member and made significant suggestions in shaping my research work, and Research Scientist, Dr. Lirong Wang, who has been mentoring me side by side to make the research scientifically sounder.

I also want to extend my appreciation to Abhishek Pandey, without whom, I couldn't have done a better job in fabricating and designing the layout. Also, would like to acknowledge the work of my fellow lab members, Shaoxu Xing, for taking care of electronic side, Changwei Liang, for participating in every discussion related to modelling side of the project, Shifeng Yu, Shuyu Wang,You Wu, and Shubin Chen for their enormous help in the field testing.

Last but not the least, I want to thank both my parents, without whom, I could never have made it. Their consistent support, dedication and all the compromises have been the reason of my strength and determination.

## Dedication

To my Parents

Mr. & Mrs. Dhruv Narayan & Sudha Todaria

And

To my Brother

Shikhar Todaria

This humble work is a sign of my love to you!

“The scientific man does not aim at an immediate result. He does not expect that his advanced ideas will be readily taken up. His work is like that of the planter - for the future. His duty is to lay the foundation for those who are to come, and point the way”

- Nikola Tesla
  (10 July 1856 – 7 January 1943)
  Electrical and Mechanical Engineer

# Contents

**List of Figures**

**List of Tables**

# Nomenclature

| | |
|---|---|
| $h$ | Height of the speed bump [m] |
| $L_1$ | Length of the first slope [m] |
| $L_2$ | Length of the flat surface [m] |
| $L_3$ | Length of the down slope [m] |
| $x_b$ | Speed bump cover stroke [m] |
| $\dot{x}_b$ | Speed bump cover vertical velocity [m/s] |
| $\ddot{x}_b$ | Speed bump cover vertical acceleration [m/s$^2$] |
| $f_n$ | Natural frequency of vibrating speed bump cover [s$^{-1}$] |
| $K_b$ | Harvester total spring stiffness [N/m] |
| $M_b$ | Mass of the speed bump cover [kg] |
| $M_{eq}$ | Equivalent mass of the harvester [kg] |
| $T_v$ | Time taken by second axle of the vehicle to reach the speed bump [s] |
| $C_b$ | Equivalent damping of the harvester [N.s.m$^{-1}$] |
| $I_{p1}$ | Inertia of the first pinion gear |
| $I_{p2}$ | Inertia of the second pinion gear |
| $n$ | Gear ratio |
| $I_s$ | Inertia of the harvester shaft |
| $R$ | Radius of the harvester shaft [m] |
| $I_g$ | Inertia of the generator |
| $R_i$ | Internal resistance [ohm] |
| $R_o$ | External resistance [ohm] |
| $V_g$ | Electromotive voltage [V] |
| $K_g$ | Electromotive voltage constant |
| $\theta_g$ | Angular rotation of the generator shaft [rad] |
| $\dot{\theta}_g$ | Angular velocity of the generator shaft [rad/s] |
| $T_g$ | Torque of the generator shaft [N-m] |
| $I_g$ | Current in the generator [A] |
| $K_t$ | Torque constant |
| $\theta_{p1}$ | Angular displacement of first pinion gear [rad] |
| $\theta_{p2}$ | Angular displacement of second pinion gear [rad] |
| $\dot{\theta}_{p1}$ | Angular velocity of first pinion gear [rad/s] |
| $\dot{\theta}_{p2}$ | Angular velocity of second pinion gear [rad/s] |

| | |
|---|---|
| $\ddot{\theta}_{p1}$ | Angular acceleration of first pinion gear [rad/s$^2$] |
| $\ddot{\theta}_{p2}$ | Angular acceleration of second pinion gear [rad/s$^2$] |
| $\theta_b$ | Angular displacement of coupling [rad] |
| $\dot{\theta}_b$ | Angular velocity of coupling [rad/s] |
| $\ddot{\theta}_b$ | Angular acceleration of coupling [rad/s$^2$] |
| $T_1$ | Torque on first pinon gear [N-m] |
| $T_2$ | Torque on second pinon gear [N-m] |
| $T_c$ | Torque on coupling [N-m] |
| $K_{c1}$ | Stiffness for first one way clutch [N/m] |
| $K_{c2}$ | Stiffness for second one way clutch [N/m] |
| $C_{c1}$ | Damping co-efficient for first one way clutch [N.s.m$^{-1}$] |
| $C_{c1}$ | Damping co-efficient for second one way clutch [N.s.m$^{-1}$] |
| $F$ | Representation of force exerted on the speed bump by moving vehicle [N] |
| $C_b$ | Equivalent electrical damping [N.s.m$^{-1}$] |
| $M_t$ | Total mass including equivalent mass and speed bump cover mass [kg] |
| $M_s$ | Sprung mass for quarter car model [kg] |
| $M_u$ | Un-sprung mass for quarter car model [kg] |
| $x_s$ | Sprung mass vertical displacement [m] |
| $\dot{x}_s$ | Sprung mass vertical velocity [m/s] |
| $\ddot{x}_s$ | Sprung mass vertical acceleration [m/s$^2$] |
| $x_u$ | Un-sprung mass vertical displacement [m] |
| $\dot{x}_u$ | Un-sprung mass vertical velocity [m/s] |
| $\ddot{x}_u$ | Un-sprung mass vertical acceleration [m/s$^2$] |
| $x_t$ | Displacement input to quarter car [m] |
| $\dot{x}_t$ | Velocity input to quarter car [m/s] |
| $K_s$ | Sprung mass spring stiffness [N/m] |
| $K_u$ | U-sprung mass stiffness [N/m] |
| $C_s$ | Sprung mass damping co-efficient [N.s.m$^{-1}$] |
| $L_f$ | Distance of the front section from the center of gravity in half car model [m] |
| $L_r$ | Distance of the rear section from the center of gravity in half car model [m] |
| $x_s$ | Sprung body mass vertical displacement in half car model [m] |
| $x_1$ | Displacement input to the front tire in half car model [m] |

| | |
|---|---|
| $\dot{x}_1$ | Velocity input to the front tire in half car model [m/s] |
| $x_2$ | Displacement input to the rear tire in half car model [m] |
| $\dot{x}_2$ | Velocity input to the rear tire in half car model [m/s] |
| $x_{11}$ | Vertical displacement of the front tire [m] |
| $\dot{x}_{11}$ | Vertical velocity of the front tire [m/s] |
| $\ddot{x}_{11}$ | Vertical acceleration of the front tire [m/s$^2$] |
| $x_{21}$ | Vertical displacement of the rear tire [m] |
| $\dot{x}_{21}$ | Vertical velocity of the rear tire [m/s] |
| $\ddot{x}_{21}$ | Vertical acceleration of the rear tire [m/s$^2$] |
| $x_{12}$ | Vertical displacement of the front section of sprung mass [m] |
| $\dot{x}_{12}$ | Vertical velocity of the front section of sprung mass [m/s] |
| $\ddot{x}_{12}$ | Vertical acceleration of the front section of sprung mass [m/s$^2$] |
| $x_{22}$ | Vertical displacement of the rear section of sprung mass [m] |
| $\dot{x}_{22}$ | Vertical velocity of the rear section of sprung mass [m/s] |
| $\ddot{x}_{22}$ | Vertical acceleration of the rear section of sprung mass [m/s$^2$] |
| $K_{t1}$ | Front tire stiffness in the half car model [N/m] |
| $K_{t2}$ | Rear tire stiffness in the half car model [N/m] |
| $K_{s1}$ | Front suspension stiffness [N/m] |
| $K_{s2}$ | Rear suspension stiffness [N/m] |
| $C_{t1}$ | Front tire damping co-efficient [N.s.m$^{-1}$] |
| $C_{t2}$ | Rear tire damping co-efficient [N.s.m$^{-1}$] |
| $C_{s1}$ | Front damping co-efficient [N.s.m$^{-1}$] |
| $C_{s2}$ | Rear damping co-efficient [N.s.m$^{-1}$] |
| $M_{t1}$ | Front tire mass [kg] |
| $M_{t2}$ | Rear tire mass [kg] |
| $M_s$ | Sprung body mass [kg] |
| $I_s$ | Moment of inertia for the sprung mass |
| $\theta$ | Pitch angle made by sprung body mass [degree] |
| $V$ | Horizontal velocity of the vehicle [m/s] |
| $x_{b\max}$ | Maximum speed bump stroke [m] |
| $I_f$ | Moment of inertia of flywheel |
| M | Mass of flywheel [kg] |
| $R_f$ | Radius of flywheel [m] |

# 1 Introduction

## 1.1 Motivation: The bigger picture

In today's world, we want to have an environment where driving is more fun, intelligent, sustained and smart. From the age of electrical based traffic lighting to the smart traffic lighting system [1]- [2], humans are experience an unprecedented level of technological advancements in the field of transportation and it is also an attempts to reducing the carbon foot print [3]. Intelligent Transportation System (ITS) is the category under which lot of researchers around the world are attempting to make the transportation more reliable, intelligent, and smart[4]- [5]. A significant research has been done, for example, on the intelligent traffic lighting. In a research, the author, Shilpa S. Chavan, suggests a microcontroller/microprocessor based intelligent traffic controls lights[6]. It serves a phenomenal solution to the traffic problems associated in a city.

On the other hand, smart road concept is a new technology that combined the transportation with artificial intelligence. For example, the use of video camera for incident detection on roads[7]. Another breakthrough research suggesting the smart road and smart car concept is done by J.Malik and his co-authors where they applied computer vision for intelligent vehicle highway system[8]. They use the computer vision for the traffic surveillance, traffic detection etc..

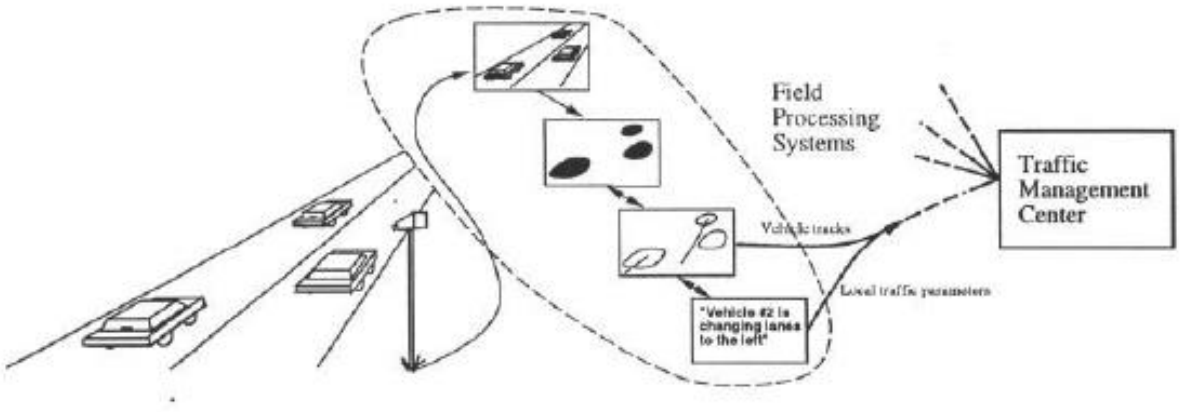


Figure 1-1 vehicle tracking system as suggested by J. Malik and his co-authors under the smart road concept[8]

Another research done by Maria Jokela etc. suggests an optical method of detecting the condition of the roads[9]. This is also used for detecting animals on the roads for preventing mishaps. They use an INR camera and thermal imaging system for this purpose. In one of the researches done by Marcin Karpi´ nski, Aline Senart and Vinny Cahill, smartly proposes a wireless sensor network on road, or, as they called it, "cat's eye" [10]. This is precisely one of the areas of application of speed bump energy harvester where it can contribute to the ITS and smart roads concept.

For all these purposes, we require an immense network of various on road sensors, wireless technology, and a robust method of powering these electronic devices. A step towards the intelligent transportation system and smart road concept, require electrical energy and it is really important to understand the limitations and constraints of the conventional sources of energy generation. Our aim is to make the ITS more independent in real sense. Another matter of concern is how we are going to provide electrical power to keep it working independently.

As we know that that electrical energy, in today's world, has a vital role in every human being's life. We simply can't imagine a world without it. From large scale to Nano –scale electricity, we are imbibed in the ways of producing more and more energy out of everything that a man can think of because every single human being on this planet deserves his share of electricity. It was projected by the international energy outlook (IEO), in 2013, that the energy consumption of the world will grow by 56% by 2040, of which, most will be produced by liquid sources and coal [11]. Figure 1-1(a) shows the trend of the electricity production by fuel type. With an increase in the energy consumption, we are making the humans life better and more productive. But, there is a darker side to it. It is a known fact that we are consuming our fossil fuels in order to scale up and provide electricity to masses. Climate change is real and is happening right now [12]–[15].

A lot of this climate change problem is associated with the way we are producing the electricity. It is estimated that, in 2014, most of the electrical energy produced in the US was from fossil fuel, such as coal, which accounted for 39% share. Figure 1-1(b) shows the US energy

production by fuel type[16]. Whereas, renewable sources such as hydro power, thermal, nuclear, and other similar forms accounted for 13% and nuclear energy with 20% share in the US in 2014 [17]. It is even larger in the developing big countries like India and China which produce 60% and 75%, respectively, of their total energy consumption via coal [18]–[20]. We are heavily consuming our natural resources in order to produce more and more electrical power and it is an apprehension that, in the near future, we will run out of the natural resources[9]- [10]. Thus, it has become vital to realize that we need to curb down our dependence on the natural sources for the electricity generation since it is going to impact our electricity market from region to region in different ways, not to mention, badly [23].

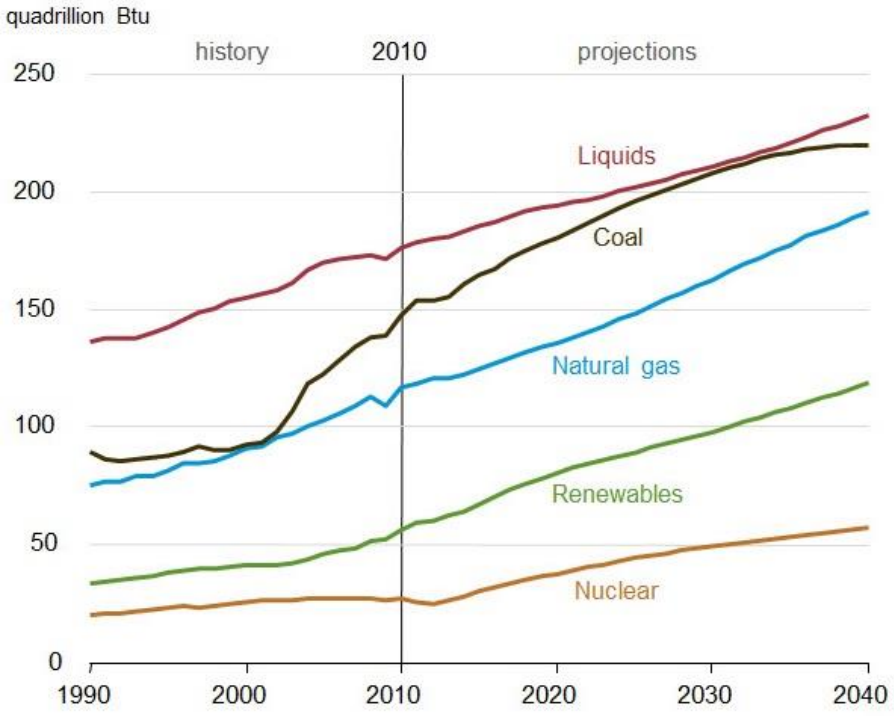


(a)

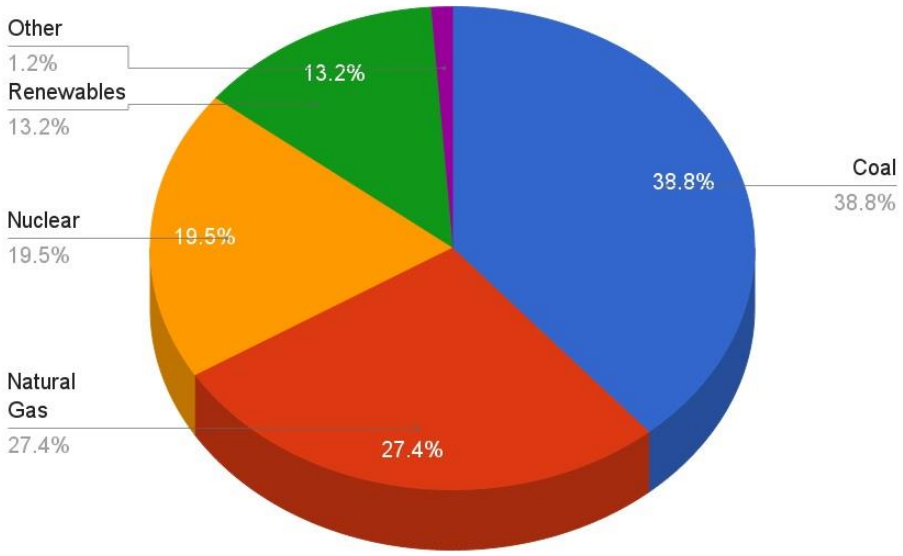


(b)

Figure 1-2 (a) Projections of the world energy consumption by IEO 2013. (b) US 2014 Electricity generation by type

In order to do so, it becomes necessary to have a paradigm shift towards the non-conventional modes of electricity generation. A lot of researchers, scientists, and engineers around the world are working towards the exploration of such methods which impose a minimum damage to our environment and, at the same time, give us clean energy. Some of the examples of such methods are wind power, gas turbine, and, most widely known, solar power which was produced less than 1% of the of the total need in 2014 [17]. There are many forms non-conventional and alternate ways of energy generation which we can and now have started trapping in order to full fill the gap for our need and to reduce the carbon footprint in the world.

Such a source of energy harvesting, which now can be synthesized, is through vehicles. With the increase in the number of vehicles on road, there is immense potential in trapping their potential and kinetic energy which can serve the purpose of small scale electrical power generation enough to make the transportation more intelligent and independent. This is called energy harvesting from running vehicle. In 2015, there were estimated 257.9 million passenger vehicles in United States[24] which can be an immense source of energy harvesting, thus, saving millions and billions of dollars in energy sector. On board/vehicle energy harvesting is coming to light these days. With regenerative shock absorbers[25] to MMR based shock absorbers[26]–[31], this area

is proving to be a promising field. Hence, a technique that can used to harvest energy outside the vehicle but using the vehicles dynamics, sounds a very interesting thought.

## 1.2 Research Objectives

The primary objectives of this research are to;

1. Provide a platform for ITS and smart road concept, which is, to be able to drive various on road electrical and electronic devices and making transportation more independent and smarter.
2. Reducing the dependence on the conventional sources of electrical energy generation at least in the transportation sector.
3. Explore current scenario of speed bumps and to give a scientific method to develop energy harvester that is able to produce large scale electrical power.
4. Keep the primary function of the speed bump, which is to reduce the speed of the vehicle on road, and at the same time, harvest significant amount of energy.
5. Give a scientific methodology to build such a harvester with supported theoretical modelling, simulation and experimental results.
6. Push the study of speed bumps/humps to make it more attractive and exploring the way which can increase its functionality.

## 1.3 Thesis Organization

The motivation and organization of the thesis are included in chapter 1. Background and the literature review including history of speed bumps, applications, its effects on vehicle dynamics, and previous works on the speed bump had been discussed in detail in chapter 2. Chapter 3 covers the details design of speed bump and energy harvester. The theoretical modelling has been introduced and discussed in detail in chapter 4. Chapter 5 introduces the experimental setup for a lab test and on road test. Results of chapter 4 and 5 have been discussed in chapter 6 of the thesis. Next, conclusion and future works has been discussed in chapter 7.

# 2 Background and Literature review

## 2.1 Speed bump and speed humps

Speed bumps/humps are a common traffic calming device that uses vertical deflection to slow down vehicles in order to improve traffic safety [32]. Geometrically speaking, speed bumps/humps are an elevated profile on the road defined by its base length, height and width. As described by Parkhill and his co-authors in the "Updated Guidelines for the Design and Application of Speed Humps" [33], "A speed bump is a raised pavement area across a roadway. Speed bumps are typically found on private roadways and parking lots and do not tend to exhibit consistent design parameters from one installation to another. Speed bumps generally have a height of 3 to 6 inches (76 to 152 mm) with a travel length of 1 to 3 feet (0.3 to 1 m)".

On the other hand, they mention, "a speed hump is also a raised area in the roadway pavement surface extending transversely across the travel way. Speed humps are sometimes referred to as "pavement undulations" or "sleeping policemen". Most agencies implement speed humps with a height of 3 to 3.5 inches (76 to 90 mm) and a travel length of 12 to 14 feet (3.7 to 4.3 m). Speed humps are generally used on residential local streets. From an operational standpoint, speed humps and bumps have critically different impacts on vehicles. Within typical residential operational speed ranges, vehicles slow to about 20 mph (32 km/h) on streets with properly spaced speed humps. A speed bump, on the other hand, causes significant driver discomfort at typical residential operational speed ranges and generally results in vehicles slowing to 5 mph or less at each bump".

They have given a clear instruction on what to be called a speed bump and hump and their clear differences. According to them, their functioning and area of installation varies. Speed bumps, as they mentioned, is a narrow width, sharply inclined profile, whereas, speed bumps are long width and have lower angle of slope making it convenient for the usage in the residential and public areas. Both have their advantages and disadvantages over each other and hence, suitable for a specific purpose on the streets and the highways.

## 2.2 Traffic calming and Speed bump/hump history

Although, the history of speed bumps/humps is not much clear to us, one of the earliest known usages of speed bump was reported in 1906, in the town of Chatham, New Jersey, United States, as a raised crosswalk 5 inches above the road [34]. Arthur Holly Compton, Nobel Laureate in physics, is one of the earliest known people who actually came up with the forerunning design of present day speed bump profile, which was more gentle, elongated, and ramped in nature [35]. He called it the “Holly hump” in 1953. Ever since, the usage of speed bumps have become a common practice across the world and it has been effectively used to reduce the average speed of the vehicles in areas where human traffic interaction is high.

As traffic logic suggests[36] , In Europe, the traffic calming began in around 1960s Frustrated by cut-through traffic rendering their streets unsafe, residents of the Dutch city of Delft turned their street into an obstacle course for motor vehicles and a safe haven for their children. This first traffic calming solution, called "living yards", or "Woonerven", slowed traffic and lessened volume with the placement of tables, benches, sand boxes, and parking bays extending into the streets. Woonerven were endorsed by the government nearly a decade later in 1976.

In the following years, the idea spread to other countries around the world. Regulations and laws were created to govern the dimensions and locations of the woonerf designs. By 1990, myriads of streets in countries such as Austria, Denmark, France, Germany, Israel, Japan, Sweden, and Switzerland were similarly calmed.

While effective for small low-volume streets, the woonerf designs slowed vehicles to 9 mph and were thus impractical for larger and more frequently traveled roads. The theory of employing physical measures to deter vehicle speed had already proven effective and experimentation began to conceive of similar ideas that would be less costly and more adaptable to larger streets. Two types of measures were considered in addition to Woonerven; diversions such as street closures or one-way streets and physical deterrents such as speed humps and similar traffic calming measures. These traffic calming measures were judged to be the most efficient and cost-effective of the three alternatives.

Even though, the history of speed bump is long enough, not too much has been thought about harvesting energy out of them. However, an extensive study on its shape, profile, and effects on vehicle dynamics and road handling has been done in the past several decades making it one of the important areas of study among the researchers and engineers working in the area of vehicle dynamics.

## 2.3 Profile and design of speed bumps/humps

There are different kinds of profiles and shapes of speed bump available in the market for the commercial usage as mentioned previously. LaToya Johnson and A.J. Nedzesky, in their study done in 2003 [37], excellently compared different shapes of common speed hump profiles. According to them, most common shapes of speed humps, also true in case of bumps, are circular, parabolic and flat topped as shown in the Figure 2-1.

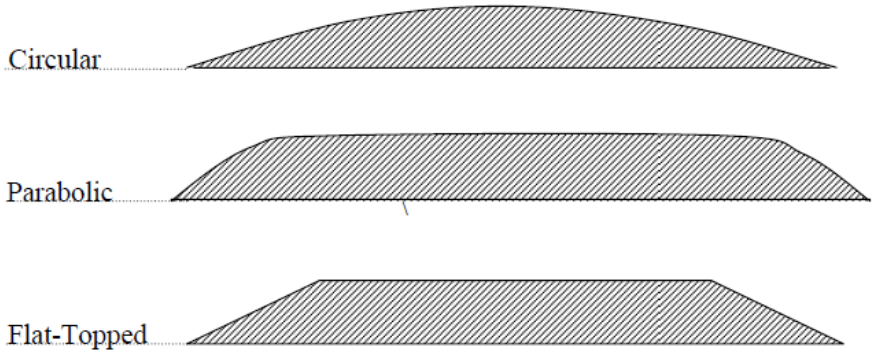


Figure 2-1 Different common speed bump and hump profiles [37]

Having different impacts on the vehicles and usages, speed bumps/humps have evolved with the course of time and due to extensive research done in the area of interaction of vehicles and the speed bumps/humps. Different profiles and shapes have been studied to find the impact on the vehicle dynamics. Moreover, There are numerous attempts made to optimize the shape and size of the hump in order to reduce the impact on the driver and the vehicle.[38]–[46]

## 2.4 Speed bump effect on vehicle dynamics

It has been widely talked that different shapes and profile of the speed bumps causes

different changes in vehicle dynamics and effects the passenger accordingly. On one side, speed bumps/humps effectively calm traffic speed to protect pedestrians, on the other side, it may cause vehicle damage and passenger discomfort. Detailed study shows that the vehicles travelling faster on a bump and cause backbone damage to the passenger [47]. The ride comfort is a very important issue when it comes to speed bump design and analysis. As concluded by, Smith, McGhee and Haley, in their report, "The prediction of passenger riding comfort from acceleration data", 1976, [48] the values of these magnitude weighted rms values ranges roughly from 0 to 0.04 g for smooth (interstate highway) rides, 0.04 to 0.06 g for medium rides, and above 0.06 for rough rides. In Sweden, an evaluation of spinal stress in bus drivers against ISO 2631-5 suggests that a bus driver shall encounter less than 150 bumps in a day at the maximum speed 10 km/h (6.25 mph) [49].

On the other hand, extensive research has been done on effectiveness of the speed bump on velocity control of the vehicle. Studies show that, by and large, speed bumps are the most effective way to control the velocity of the moving vehicles on the road [50], [51]. Alongside this, there have been various attempts to showcase the effects of speed bumps/humps and cushions on the handling of the vehicle[52], [53].

### 2.5 Energy harvesting sources

Energy harvesting is the field where the electrical energy is trapped from the surrounding operating environment. As described by Priya and Inman in Energy Harvesting Technologies, [54] ,there are basically three energy harvesting sources, piezoelectric, thermoelectric and electromagnetic energy. Among these three energy harvesting sources, piezoelectric and thermoelectric have widely been explored and discussed in the literature[54]. There are several instances in the news where people have used piezoelectric devices on the road and speed bump in order to generate electrical energy [55], [56]. Whereas, Andriopoulou Symeoni in his research, showcased the way to harvester energy from roads using thermoelectric devices[57]. However, in both piezoelectric and thermoelectric harvesting techniques, the scope of energy generation is very limited, maximum to the scale of micro watts. Hence, it can't be a replacement of conventional sources of energy generation. Of these three sources, the most promising source seems to be electromagnetic energy harvesting which is capable of generating significant amount of electric energy which could be used for various applications. Surprisingly, not much has been done in this area except some independent companies and researchers have done harvesting from speed bumps

and roads using electromagnetic generator and simple mechanical crankshaft motion [58]–[65] but, either they lack the scientific approach or simply the energy produced in their concept is not sufficient to supplement the existing infrastructure. In another research done by Zhang [66], the use of linear generator to produce large scale electrical power is pretty impressive but its area of implementation is in the tunnels and highway and still lacks much power to run road side electrical equipment.

In this research, both effectiveness and amount of power generated is significant and can supplement and support the existing infrastructure. To summarize, when a vehicle touches a speed bump, the speed bump receives the impulsion energy transferred from vehicle, which provides one possible energy source to be regenerated to power road-side devices. Harvesting the vibration energy from speed bumps may become a valid solution in some areas where grid electricity is economically unavailable for applications such as, to power traffic lights, warning sign or traffic sensors. The theoretical results show us that the project is capable of achieving an electrical output of more than 1 KW

# 3 Design of Speed bump energy harvester

## 3.1 Area of installation

The speed bump energy harvester is primarily designed to harvest energy from the vehicles clocking in and out of the administrative parking lot of the State university of New York at Stony Brook, NY. Since, it was to be installed in the parking lot, speed bump was suitable for the purpose. The goal was to reduce to speed of the vehicle entering and exiting the parking lot below 15 miles/hour and at the same time generating electrical energy which would be used for various clock in/out devices such as monitoring camera, shutter gate and various other monitoring sensors. However, the research was conducted in a very generic way and the designed harvester was suitable for the on-street power generation and applications as well.

## 3.2 Concept development

The concept of speed bump energy harvester is to absorb the kinetic and potential energy of the vehicle, while vehicle runs over the speed bump. Unlike the conventional speed bumps as defined by the Institution of Transportation Engineers[67], this concept is based upon a linearly moving speed bump which, when comes in contact with a vehicle, generates a stroke like motion, which in turns, translates the linear motion of the speed bump into rotational motion with the help of a rack and pinion gear assembly. It uses any linear motion or vibration caused by the vehicle impact onto the bump, and uses it to produce large scale electrical power. This novel speed bump harvester concept is based on the previous research in large-scale energy harvesting. In research field of large scale vibration energy harvesting, L. Zuo and etc. did pioneering investigation to regenerate large scale energy with high energy conversion mechanism which proposes a mechanical motion rectifier (MMR) to convert linear up-down vibration into uni-directional rotation of generator to regenerate electrical power from vibration of vehicle absorber and ocean wave [26]–[29], [31], [68]. The design presented in the paper is the forerunning concept of the MMR system and is used in this research of speed bump energy harvesting. This project uses the same technique to increase the overall energy generation capacity. MMR is discussed in details in the later section of energy harvesting module.

The concept development phase is described in the following flow chart in Figure 3-1. The prototype is broken into 4 different modules which includes, Vehicle dynamics, Speed Bump, energy harvesting, and last, energy storage. The speed bump energy harvester is composed of the speed bump module and energy harvesting module. The system level design is done only to the speed bump and energy harvesting module also up to an extent, energy storage module. Vehicle dynamics module, being an input, is kept as a variable.

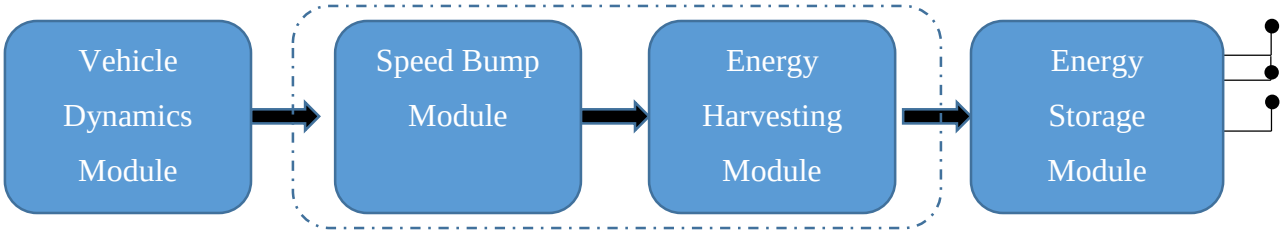


Figure 3-1 Schematics of the speed bump energy harvester

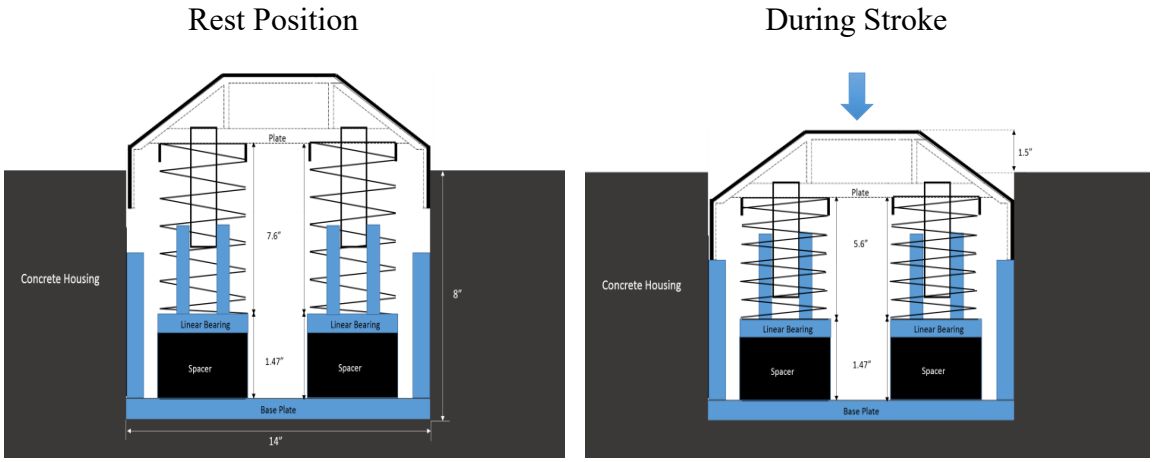


Figure 3-2 Motion of the speed bump energy harvester during resting position and stroke

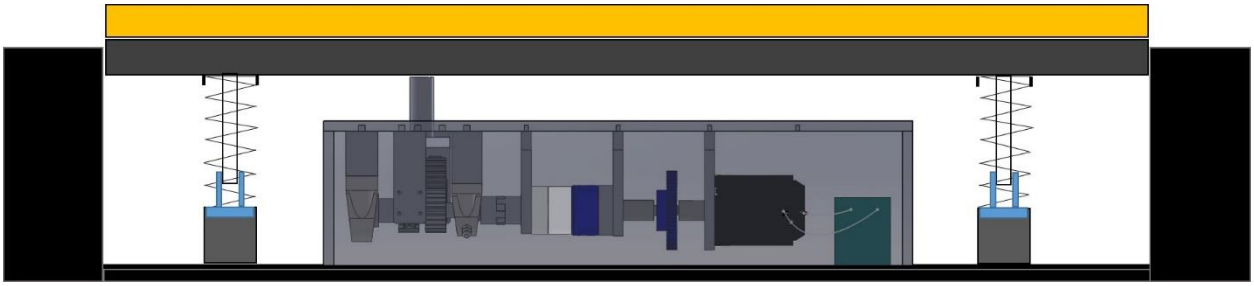

Figure 3-3 Side view of the speed bump energy harvester combined with the speed bump module

Figure 3-4 A common car on commercial circular speed bump

## 3.3 Speed bump energy harvester system design, 3-D modelling & prototype

The proposed speed bump energy harvester is made up of various smaller components which are assembled in order for it to function. There are two main part or modules of speed bump energy harvester which are separated according to their functionality. First, the energy absorber or the speed bump cover and, second, the energy harvester. These two main modules further have smaller units which are discussed in detail in the following section.

### 3.3.1 Speed bump module

This module includes the speed bump cover, the connecting rod, speed bump cover base, linear bearings, linear bearing blocks, linear shafts and most important, springs. All these parts of the module bear most of the heavy loads which is set upon the system. This module is responsible for diverting the potential and kinetic energy of the vehicle to the harvesting module which is then used for energy harvesting purpose. Among all these parts, speed bump cover, connecting rod, linear shafts, and, linear bearing blocks, base plate are fabricated in the machine shop and linear bearings and springs are procured according to the estimated calculations.

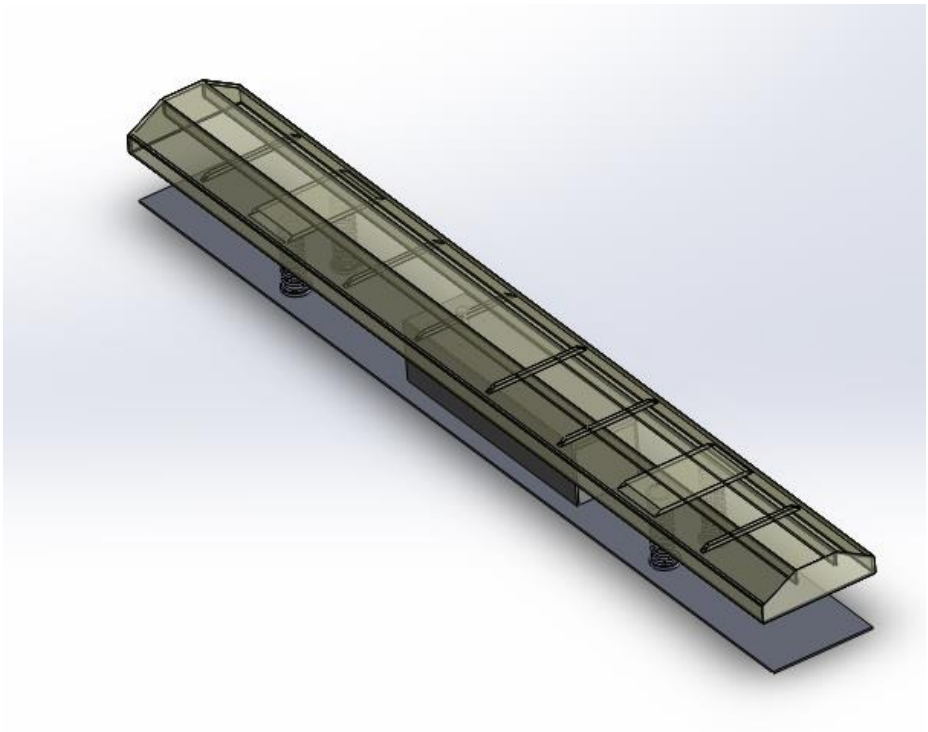

(a)

(b)

Figure 3-5 (a) 3-D model of speed bump energy harvester (b) real prototype of the speed bump energy harvester

3.3.1.1 Speed bump cover

Speed bump cover profile is chosen to be flat topped, which is one of the most common shapes for the speed bumps, with a height, *h*, of 3.5 in (0.0889 cm), length of 9 ft and width or cross sectional length, $L\ (L_1+L_2+L_3)$, of 14.5 in. Cast iron is used for building the prototype with three rectangular shaped sheets of 0.2 in thickness, welded together with adjacent angle of 150 degree from the top plate giving it a flat topped shape. Mass of the speed bump is 150 kilograms. Figure 3-5 (a), (b) illustrates the 3-D design and fabricated speed bump cover underneath which springs and energy harvesting unit is kept. Figure 3-6 (a), (b) and Figure illustrates the cross sectional 2 D drawing and top view 3-D model of the speed bump cover.

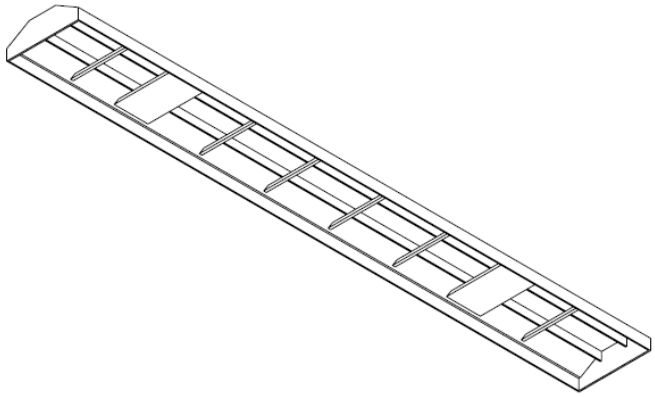

(a)

(b)

Figure 3-6 (a) speed bump cover 3-D drawing (b) inner view of the fabricated speed bump cover

3.3.1.2 Connecting rod

The only link between the two modules and is responsible for transferring the load of the vehicle to the harvesting module. At time of action, the entire load is carried by this connecting rod and thus, made of stainless steel 440 in order to withstand the shock and carrying load effectively. The length of the connecting rod is set at 5 in.

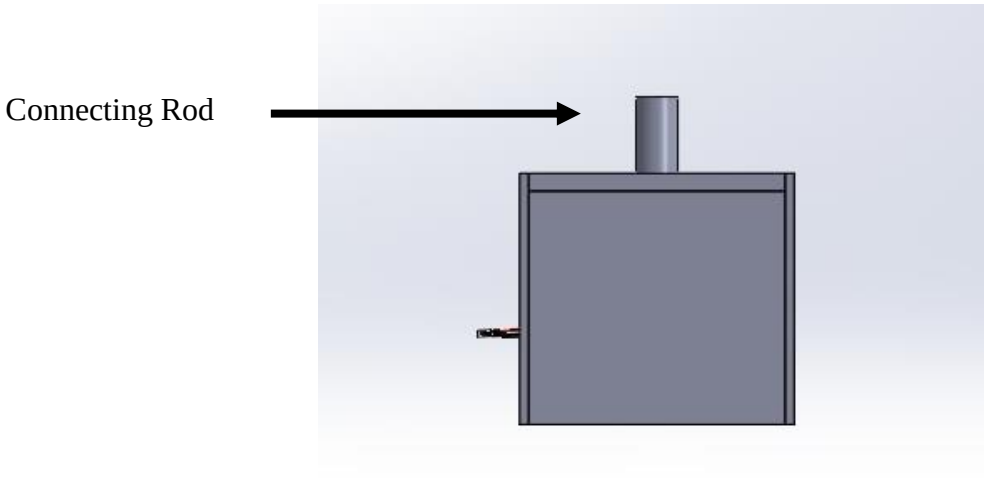


Figure 3-7 Front view of speed bump energy harvester casing showing the connecting rod on the top

3.3.1.3 Speed bump cover base

It is a thin plate of aluminum with 0.25 in of thickness and along with length of the plate, rectangular ribs are welded across the length plates in order to give it more bending stiffness.

3.3.1.4 Linear bearings and shafts

The speed bump cover freely rests on the springs and to provide it a linear movement, linear shaft and the linear bearings, which rest on the bearing blocks, are used. Since, linear shafts have to withstand heady loads, the material chosen for it is 440 stainless steel which is same material as being used for connecting rod.

Figure 3-8 Linear bearings assembled within mounting blocks, springs, supporting shaft, base plate, and speed bump cover


Figure 3-9 linear shafts mounted on the speed bump cover as a linear guide. Cross sectional rids welded across the cover to give strength to it

3.3.1.5 Springs and its selection

Spring selection is one of the most critical parts of the system design process since it determines the proper functioning, load capacity and self-generating capacity of the speed bump energy harvester. The time for speed bump to rebound to its original position can be estimated by a quarter period of time according to its natural frequency. The natural frequency of speed bump can be expressed as

$$f_n = \sqrt{\frac{k_b}{(m_b + m_e)}} \tag{1}$$

Where $f_n$, $k_b$, $m_b$, and $m_e$ will be the natural frequency of speed bump, spring stiffness, mass of speed bump and the equivalent mass of energy harvester, which will be introduced in the later section. Assuming that the time between the front and rear axles of vehicle passing through the speed bump is $T_v$, then

$$\frac{1}{(4 \cdot f_n)} \leq \frac{1}{f_v} = T_v \tag{2}$$

Substitute Eq. (1) into (2),

$$k_b \geq \frac{(m_b + m_e)}{T_v^2 16} \tag{3}$$

The time, $T_v$, can be calculated according to vehicle speed and axle distance. Moreover, larger the equivalent mass of harvester, larger stiffness of the spring should be.

Figure 3-10 springs supporting speed bump cover

### 3.3.2 Energy harvesting module

Energy harvesting module comprises of several small and critical components such as rack and pinion gear system, gear box, Brushless DC motor/generator, couplings, bearings, and the most important, one way clutches, which help achieving the mechanical motion rectification. The details of the energy harvesting module components are discussed in the following sections

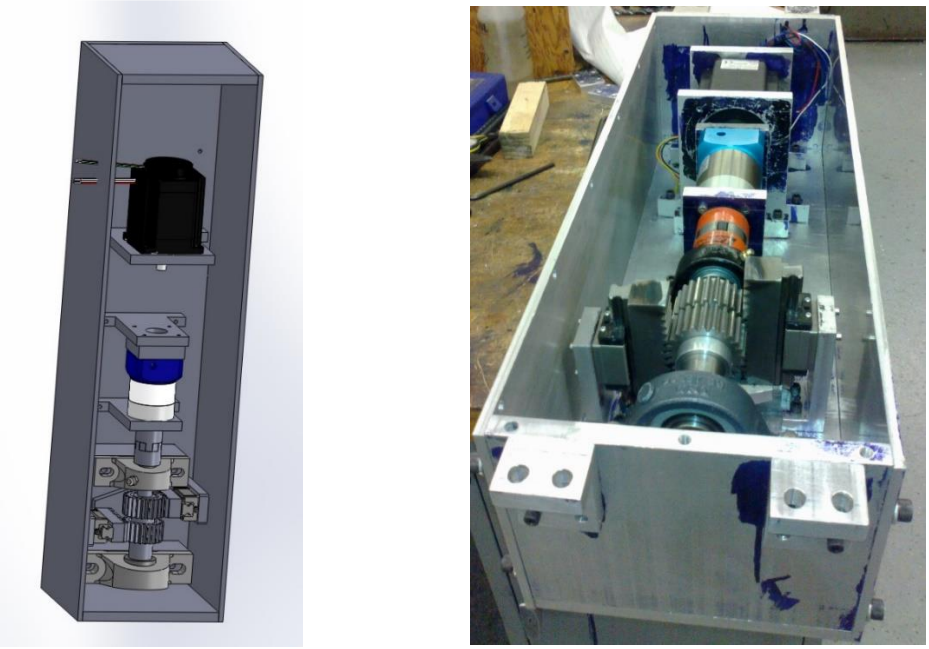

Figure 3-11 (left) - 3-D model of speed bump energy harvester module (right- prototype of the speed bump energy harvester module)

#### 3.3.2.1 Rack and pinion gear system

Rack and pinion gear pair provide the conversion of linear motion into rotational motion. The same assembly has been used in the prototype which will initiate the harvester's rotational movement one the vehicle's kinetic and potential energy is absorbed by speed bump cover and transferred by the connecting rod to the pair of rack gears. The figure illustrate the layout of rack and pinion gear system used in the prototype.

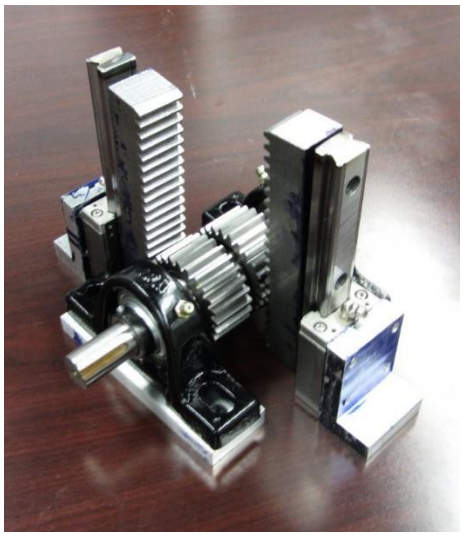

Figure 3-12 Rack and pinion gear assembly

3.3.2.2 Gear box

Gear box serves a critical function in the harvesting unit. The rotational speed of the pinion is not sufficient enough to drive the motor and thus, isn't enough to achieve the rated speed of the motor. The gear ratio, *n*, used in the prototype is 1:50. Thus, the velocity after the increase would be 50 times higher than the rotational speed of the pinion gear.

3.3.2.3 Brushless DC motor (BLDC motor)

Brushless DC motors are more efficient as there is not brushes and hence, the chances of any friction are removed. Also, BLDC motor can work as a generator and hence, a 3 phase, single shaft BLDC motor has been used for the prototype. Detailed description of the motor can be found here [69].

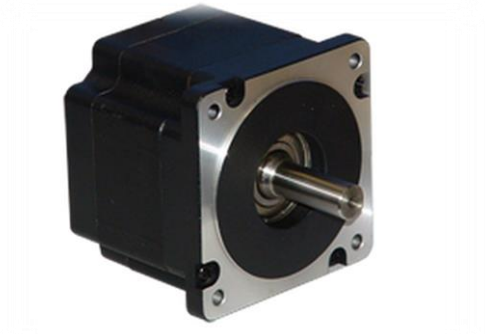

Figure 3-13 Brushless DC motor/generator

3.3.2.4 One way clutch bearings

There are several designs of one way clutch available which are patented under U.S. Patents [70]–[74]. In this research, there are 2 one-way clutches fitted with the pair of pinion gears which allow the motion of the rack to take place in two direction, but only allows shaft to rotate uni-directionally. Figure 3-14 represents the 2-D cross sectional design of a typical one way clutch with its functioning. The functioning of such a one way clutch could be found in the literature on the website. [75]

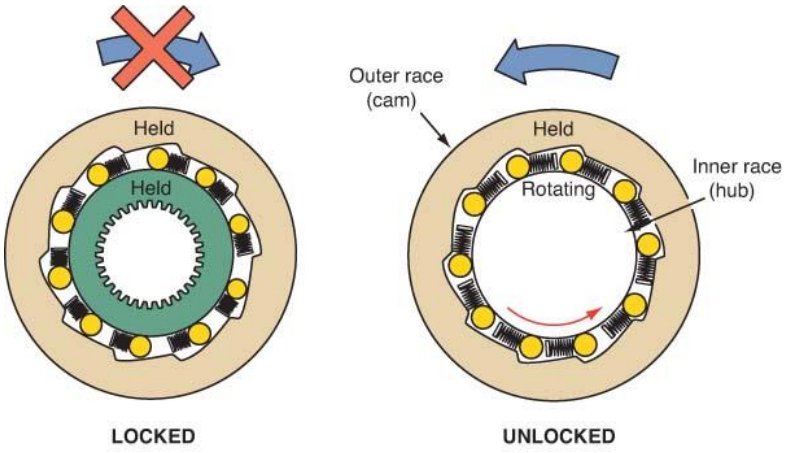


Figure 3-14 Representation of the one way clutch with its functioning [75]

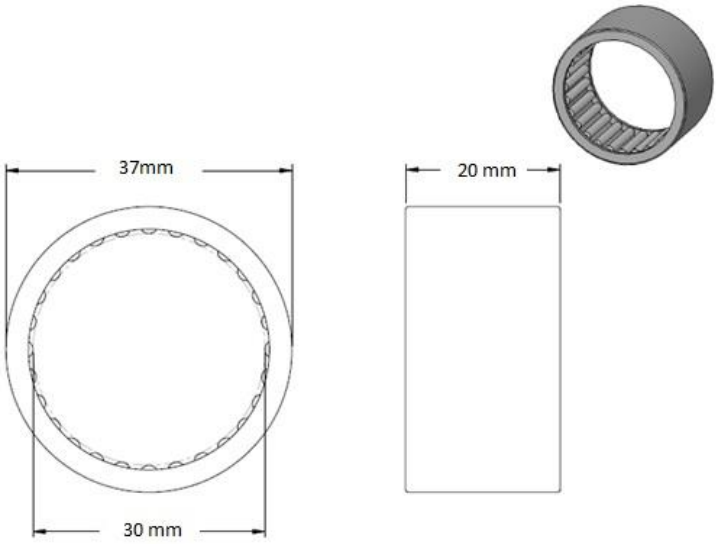


Figure 3-15 2-D and 3-D view of the one way clutch used in the prototype [76]

3.3.2.5 Harvester casing and sealing

The energy harvesting module is encased in a cuboid and sealed with sealing material to ensure that no water comes inside the electrical or mechanical part of the harvester. The cuboid is made of aluminum to avoid any kind of rust or corrosion. The connecting rod, as described in section 3.3.1.2, movies linearly through the harvesting case and it the only opening of it. In order to ensure the sealing of the hole, two O rings are placed, one at the top and the other at the bottom of the top plate of the harvester case. These O rings are specially placed in a grove cut with the same depth as the wire diameter of the O rings so that they can be placed perfectly. Then bottom and the top O rings are further fixed and sealed with the help of an aluminum plate or top seal plate. Detailed 3-D design of the harvester assembly is shown in the Figure 3-16

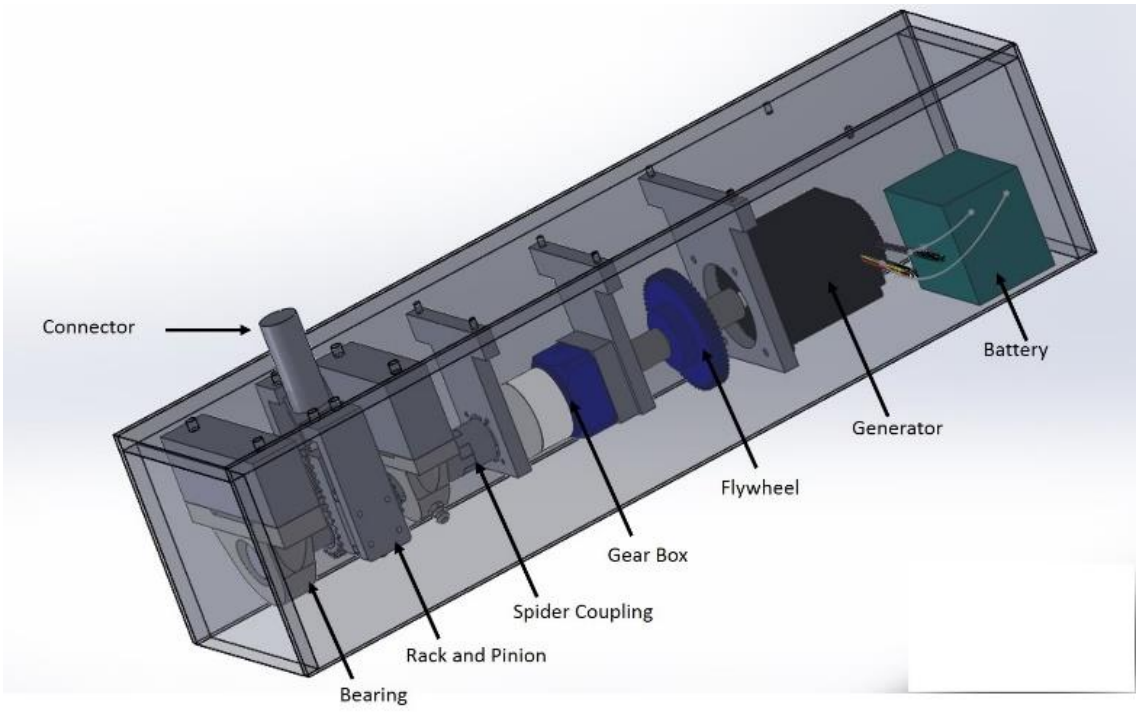


Figure 3-16 3-D assembly of the energy harvesting module indicating different parts of the assembly

Figure 3-17 to 3-19 showcases the side view, front view and the fabricated and assembled prototype of the speed bump energy harvester module

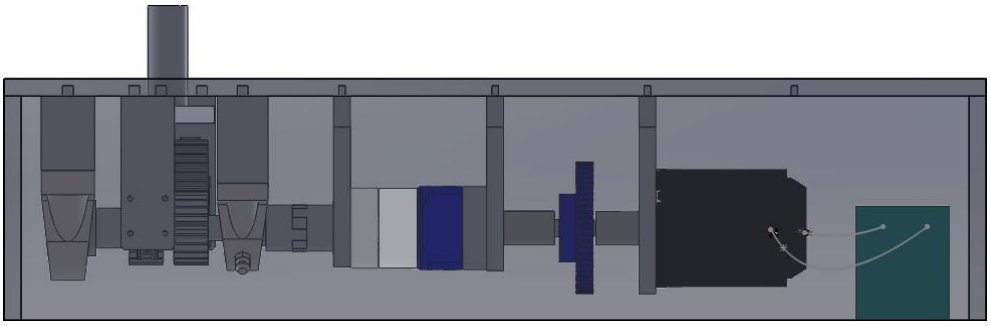

Figure 3-17 Side view of the assembly of energy harvester module

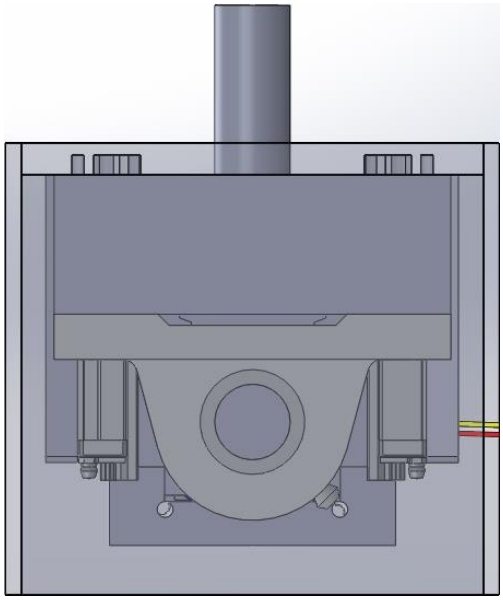

Figure 3-18 Front view of the harvester module

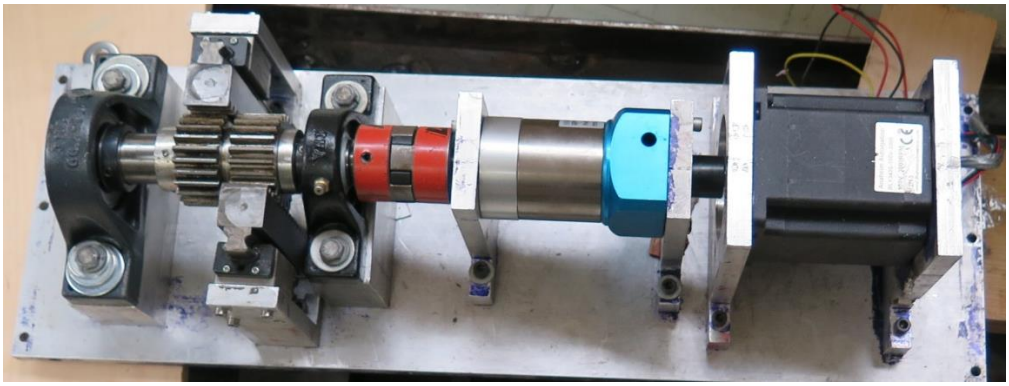

Figure 3-19 assembled prototype of the energy harvester unit

### 3.3.3 Mechanical motion rectification (MMR)

The schematics of energy conversion mechanism, as shown in Figure 3-20, which is called the mechanical motion rectifier (MMR)[30], by which the linear translational motions of two racks are converted to the rotational motion with the engagement and disengagement of the two one-way clutches. The two racks are connected with speed bump cover via the connector. When the two racks move with the speed bump cover vertically, the two pinions will rotate with the movement of racks. However, the two one-way clutches inside the pinions are installed in such a way that only one of the two clutches is engaged at an instant time to drive the shaft. When a vehicle rolls over the speed bump cover, the speed bump cover and racks are first pressed down. During this process, the first one-way clutch is engaged and drives the shaft meanwhile, the second one-way clutch is disengaged. After the tire rolls over, the speed bump and racks will move upwards under the spring force. The second one-way clutch is engaged to drive coupling shaft and the first one-way clutch is disengaged. The engagement and disengagement between the pair of one-way clutches result in the coupling shaft to be driven in the same direction, irrespective of the direction of the movement of racks. This is the working principle of the proposed mechanical motion rectifier, which is similar as the electrical voltage rectifier using center-tapped transformer. Since the rotational speed obtained by the linear motion of rack is not so high, a gear box, as described in section 3.3.2.2 is used to speed up the generator to its rated speed for energy conversion efficiency.

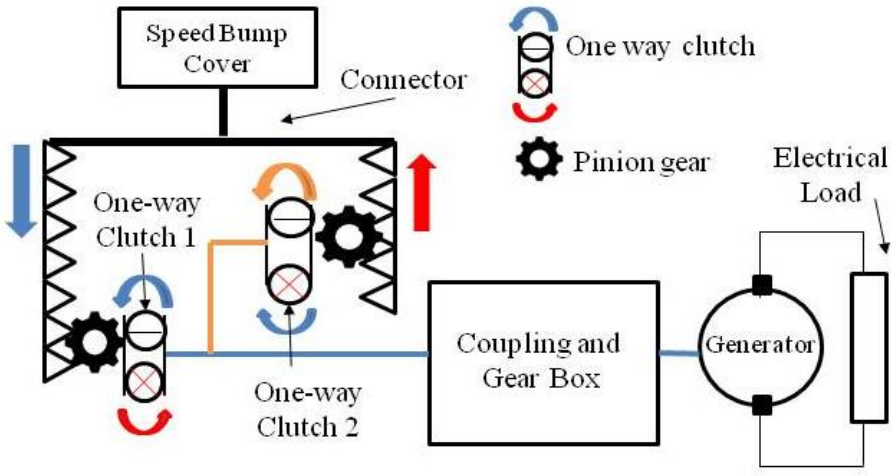


Figure 3-20 Schematics of the mechanical motion rectifier (MMR)

# 4 Analytical modelling

## 4.1 Speed bump energy harvester dynamics

As described in the previous sections, the speed bump harvester is modelled as one body mass system as illustrated in the figure. With the mass of the bump cover, mb, and equivalent mass, $M_e$, which is the inertial mass of the rotating parts.

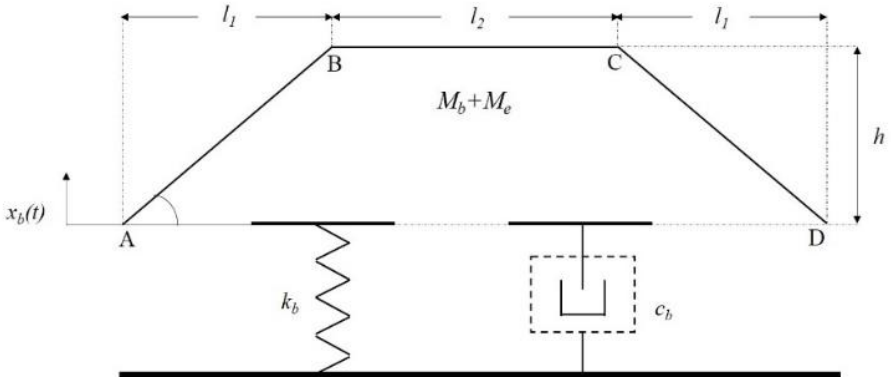


Figure 4-1 2-D speed bump energy harvester model

Where, $M_b$, $M_e$, are the masses of speed bump cover and the equivalent mass. $K_b$ and $C_b$ are the spring stiffness and the equivalent electrical damping. $X_b$ is the speed bump displacement and $h$ is the total height of the speed bump. Whereas, the schematics of the moving parts, i.e. pair of pinion gears, one way clutches, coupling, gearbox and generator is shown in Figure 4-2.

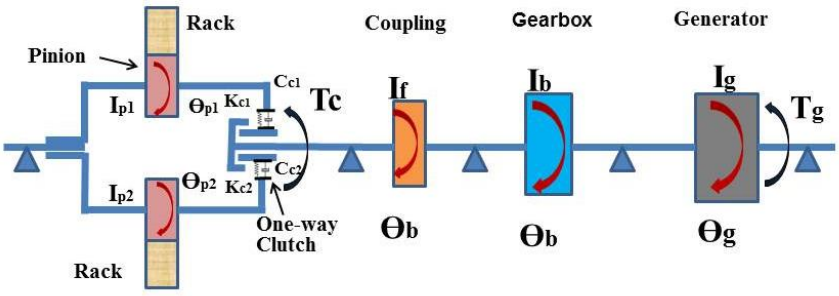


Figure 4-2 Systematic representation of the energy harvesting module

### 4.1.1 Equivalent mass

As mentioned in the previous section, Equivalent mass, $M_e$, is the inertial mass which will resist the motion of the bump cover in the beginning or in more specific words, it is the inertial mass of the rotating parts of the harvester such as gear box, coupling, motor etc. combined. Following equation is used to determine the equivalent mass of the system;

$$M_e = \frac{I_{pj} + I_s + n^2 I_g}{r^2} \tag{4}$$

Where, $I_p$, $I_c$ and $I_g$ are the inertia of pinion gears, coupling shaft and generator respectively. The $n$ is the gear ratio of gear box and $r$ is the radius of the pinion gear. So, $M_e$ is added to the mass of the speed cover, as shown in Figure 4-1, considering it to be placed at the end of the rack. It is an important parameters in defining the state of the system when the dynamics is taken into consideration. Later section describes the function of it in detail.

### 4.1.2 Equivalent damping or electromagnetic damping

Similar with the equivalent mass, equivalent damping, $C_e$, is an electrical damping caused by the electromagnetic generator. A model of the electromagnetic generator model is setup as shown in Figure 3, in which the rotational back electromotive voltage, $V_g$ ,is proportional to the rotational speed of generator shaft described as the following equation:

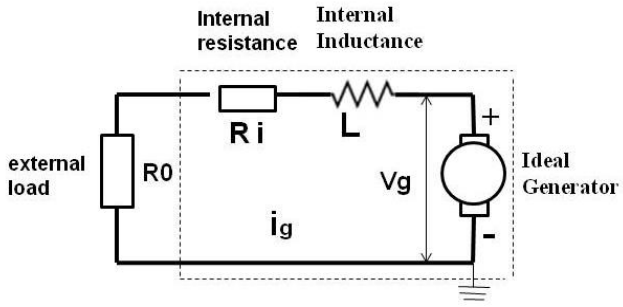


Figure 4-3 Simple electrical circuit of the generator

$$V_g = K_g \dot{\theta}_g n \tag{5}$$

Where $V_g$ , $K_g$ , $\dot{\theta}_g$ , and $n$ are the electromotive voltage, counter electromotive voltage constant, rotational speed of the generator and gear ratio respectively. Furthermore, the counter electromagnetic induced torque, which is proportional to the current as;

$$T_g = K_t \cdot i_g \tag{6}$$

Considering the equation (5), we can get

$$T_g = K_t \cdot \frac{V_g}{R_i + R_0} = \frac{K_t K_g \dot{\theta}_g n}{R_i + R_0} \tag{7}$$

4.1.3 One way clutch modelling

A dynamic model of Speed bump energy harvester, as shown in Figure 4-2, is built up according to the physical prototype in Figure 3-9. The model includes three parts:

1. Mass of top plate attached with connecting rod/rack;
2. Inertia of $I_{p1}$/ $I_{p2}$ with pinion and outer ring of one way clutch;
3. Harvester shaft with generator, gearbox, coupling and the inner shaft of one way clutch.

Here the inertia of one way clutch is neglected. The dynamic equations of these three parts are as followings:

$$M_b \ddot{x}_b + \frac{T_j}{R} = F \text{ or} \tag{8}$$

$$I_{pj} \ddot{\theta}_{pj} = T_1 - T_c \text{ or} \tag{9}$$

$$(I_s + n_b{}^2 I_g)\ddot{\theta}_b = T_c - T_g \tag{10}$$

Where j=1,2, representing the pinion gear 1 and 2 respectively, $M_r$ , $I_{pj}$ , $I_s$ and $I_g$ are the mass of rack assembly, inertia of each pinion $P_1$ and $P_2$ , inertia of coupling, gearbox and generator respectively; $x_b$ is the vertical displacement of the rack and connecting rod; $\ddot{\theta}_{pj}$ and $\ddot{\theta}_b$ are the angular acceleration of each pinion $P_1$ , $P_2$ and coupling; the angular acceleration of generator $\ddot{\theta}_g = n_b \ddot{\theta}_b$ , $n_b$ is gearbox ratio; $T_1$, $T_2$ , $T_c$ and $F$ are the torque on each pinion, one way clutch and the force loaded on the cover link rod. When one clutch is engaged and the other is disengaged, the torque on the disengaged is neglected.

The one way clutch can be modeled as a discontinuous contact model with stiffness $K_{c1}$ and $K_{c2}$, or, for representation sake, $K_{cj}$ and damping $C_{cj}$ for each one way clutch. (j=1,2). The torque on the one way clutch can be expressed as

$$T_c = K_{cj}(\theta_{pj} - \theta_b) + C_{cj}(\dot{\theta}_{pj} - \dot{\theta}_b) \tag{11}$$

where $\theta_{p1}$, $\theta_{p2}$ and $\theta_b$ are the rotational angular of the each pinion and coupling. $T_c$ is the torque to drive coupling input shaft, when one of the two way clutch is engaged respectively. One way clutch is disengaged when the driving velocity is larger than driven velocity, and it is engaged when driving velocity is smaller than driven velocity. When the damping of one way clutch is small and neglected, the torque equation can be expressed as

When one way clutch is engaged:

$$T_c = K_{c1}(\theta_{pj} - \theta_b), \quad (\dot{\theta}_{pj} - \dot{\theta}_b) \geq 0 \tag{12}$$

When one way clutch is disengaged:

$$T_c = 0, \qquad (\dot{\theta}_{pj} - \dot{\theta}_b) < 0 \tag{13}$$

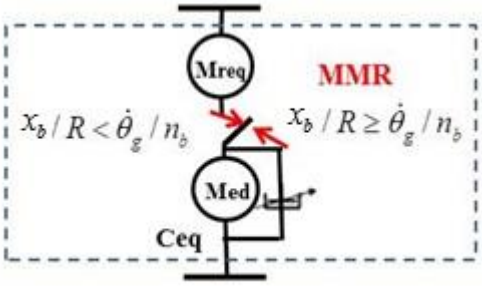


Figure 4-4 model of engagement and disengagement

The displacement, $x_b$, of rack and the angular displacement, $\theta_{p1}$, has the relationship $x_b = \theta_b r$ and $\ddot{x}_b = \ddot{\theta}_b r$, where $r$ is the radius of pinion. When one way clutches are disengaged,

the pinion shaft and generator shaft rotate together, decoupling itself with the rack and pinion with $T_c = 0$, therefore, decoupled eq. can be expressed as,

There are primarily two kinds of states which can define the dynamics of the energy harvesting system. One of engaged phase and another disengaged phase. These are defined in the following section.

### 4.1.4 Engaged harvester state

State is said to be engaged when Eq. (8) is satisfied. That means, if the pinion gear can provide an additional torque to the harvester shaft, the system will enter the engaged state. Direction of the rack does not have any role since using the pair one way clutch, we rectify the bi-directional movement of the rack and get a unidirectional rotational motion in the harvester shaft.

Hence, equation for the motion for speed bump harvester is

$$(M_r + \frac{I_{pj} + I_s + n_b{}^2 I_g}{r^2})\ddot{x}_b + \frac{K_t K_g n_b{}^2}{r^2(R_i + R_0)}\dot{x}_b = F \tag{14}$$

Where, j=1,2, representing pinion gear 1 and 2, *F*, is the force exerted by the vehicle onto the speed bump. Explanation of the force, *F*, is discussed in detail in the further sections.

$$M_t = M_b + \frac{I_{pj} + I_s + n_b{}^2 I_g}{r^2} \tag{15}$$

$$M_{eq} = \frac{(I_s + n_b{}^2 I_g)}{r^2} \quad \&, \tag{16}$$

$$C_{eq} = \frac{K_t K_g n_b{}^2}{r^2(R_i + R_0)} \tag{17}$$

Where, $M_t$, is the total mass including, mass of the speed bump $M_b$, and equivalent mass of the rotation bodies inside the harvester. Hence, Eq. (14) an be rewritten as,

$$M_t \ddot{x}_b + C_{eq}\dot{x}_b = F \tag{18}$$

### 4.1.5 Disengaged harvester state

State is said to be engaged when Eq. (8) is satisfied. That is, the instantaneous angular velocity of the pinion gear is less than the angular velocity of the shaft. This is also called the decoupled state, where, the harvester dynamics is separated from the speed bump dynamics. Therefore, the following equations govern the two individual system.

For harvester, governing equations is;

$$M_{eq}\ddot{x}_b + C_{eq}\dot{x}_b = 0 \tag{19}$$

And, for the speed bump, the governing equation is;

$$M_b\ddot{x}_b + K_b x_b = F \tag{20}$$

In the disengaged state, the energy harvested will be entirely based on the instantaneous angular velocity of the generator shaft and the decaying shaft velocity will be;

$$\dot{\theta}_g = \dot{\theta}_g e^{-\left(\frac{C_{eq}}{M_{eq}}\right)t} \tag{21}$$

To summarize the engagement and disengagement, following table as be shown;

Table 4-1Conditions for engagement and disengagement

| **Stages/State** | **Engaged State** | **Disengaged State** |
|---|---|---|
| If $0 \geq x_b > -x_{b\max}$ | $\dot{\theta}_{pj} \geq \dot{\theta}_b$ | $\dot{\theta}_{pj} < \dot{\theta}_b$ |
| If $x_b \leq -x_{b\max}$ (Bottom Stop) | Definitely disengaged Since $\dot{\theta}_{pj} = 0$ | $\dot{\theta}_{pj} = 0$ |
| If $x_b \geq 0$ (Upper Stop) | Definitely disengaged Since $\dot{\theta}_{pj} = 0$ | $\dot{\theta}_{pj} = 0$ |

## 4.2 Vehicle dynamics model

Vehicle dynamics model has been studied widely by many scholars in the past and the most famous vehicle dynamics models are quarter car, half car and full car model and in this research, all the vehicle models are taken from the literature, Vehicle Dynamics, by Reza N. Jazar [77]. Here, in our study, the preliminary work has been done on the quarter car model to validate the effectiveness of our analytical modelling. Hence, the governing equation for the quarter car model is following;

### 4.2.1 Quarter car model

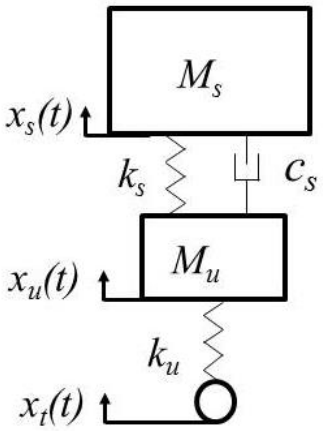


Figure 4-5 quarter car model of 2 axle vehicle

A quarter vehicle model from reference is adopted in this research as illustrated in Figure 5. Only the vertical vibration of the vehicle is considered in this research. The quarter vehicle model is a two-mass vibration system with body mass of $M_s$ and unspring mass of $M_u$. The vertical displacement of sprung and un-sprung mass is represented as $x_s$ and $x_u$ respectively. The stiffness and damping of the suspension system are described as $K_s$ and $C_s$ respectively and the stiffness of tire is indicated as $K_u$ and the damping of tire is neglected due to be smaller than that of both suspension and speed bump. The two-mass vibration system can be expressed as the following two equations,

$$M_s\ddot{x}_s + C_s(\dot{x}_s - \dot{x}_u) + K_s(x_s - x_u) = 0 \tag{22}$$

$$M_u\ddot{x}_u - C_s(\dot{x}_s - \dot{x}_u) - K_s(x_s - x_u) + K_u(x_u - x_t) = 0 \tag{23}$$

Where $\ddot{x}_s$ and $\ddot{x}_u$ are the vertical accelerations of sprung and un-sprung mass respectively, $\dot{x}_s$ and $\dot{x}_u$ are the vertical velocity of the sprung and the un-sprung mass respectively. Here $x_t$ is the movable displacement boundary input. $x_t$ will be influenced by the position of tire and speed bump cover stroke.

4.2.2 Half car model

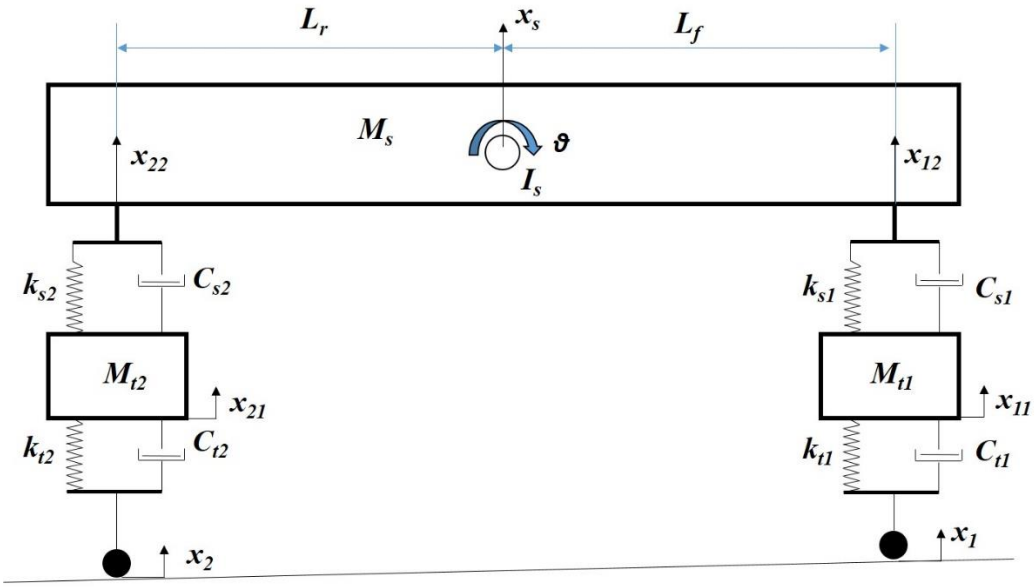


Figure 4-6 half car model of 2 axle vehicle

Above figure illustrates the half car model used in the study of vehicle dynamics. Where $x_s, \theta$ the movement of the vehicle body at gravity center; $M_s$ and $I_s$ the body mass and inertia; $L_f$ and $L_r$ the distance of center of the vehicle from the front and rear suspension, $K_{s1}$, $K_{s2}$, $C_{s1}$ and $C_{s2}$ are the stiffness and damping of the front and rear suspensions. Where $M_{t1}$ and $M_{t2}$ are the unspring mass, $K_{t1}$, $K_{t2}$, $C_{t1}$, $C_{t2}$ are the stiffness and damping of the front and rear tires respectively. $x_{11}, x_{12}, x_{21}, x_{22}$ are the vertical displacement of the front tire, front body, rear tire and rear body of the vehicle. $x_1$ and $x_2$ are the inputs to the front and the rear tire respectively.

Now, the governing equations of the half car model are the following;

For vehicle sprung mass;

$$M_s\ddot{x}_s = -K_{s1}(x_s - L_f\cdot\theta - x_{11}) - C_{s1}(\dot{x}_s - L_f\cdot\dot{\theta} - \dot{x}_{11}) - K_{s2}(\dot{x}_s - L_r\cdot\theta - x_{22}) - C_{s1}(\dot{x}_s - L_r\cdot\dot{\theta} - \dot{x}_{22}) \quad (24)$$

$$I_s\ddot{\theta} = -L_f(-K_{s1}(x_s - L_f\cdot\theta - x_{11}) - C_{s1}(\dot{x}_s - L_f\cdot\dot{\theta} - \dot{x}_{11})) + L_r(-K_{s2}(x_s + L_r\cdot\theta - x_{22}) - C_{s2}(\dot{x}_s + L_r\cdot\dot{\theta} - \dot{x}_{22}) \quad (25)$$

For vehicle un-sprung masses;

$$M_{t1}\ddot{x}_{11} = -K_{s1}(x_{11} - x_s + L_f\cdot\theta) - C_{s1}(\dot{x}_{11} - \dot{x}_s - L_f\cdot\theta) - K_{t1}(x_{11} - x_1) - C_{t1}(\dot{x}_{11} - \dot{x}_1) \quad (26)$$

$$M_{t2}\ddot{x}_{22} = -K_{s2}(x_{22} - x_s + L_r\cdot\theta) - C_{s2}(\dot{x}_{11} - \dot{x}_s + L_r\cdot\theta) - K_{t2}(x_{22} - x_2) - C_{t2}(\dot{x}_{22} - \dot{x}_2) \quad (27)$$

## 4.3 Dynamics of the combined speed bump energy harvester and vehicle model

### 4.3.1 Speed bump modelling with quarter car dynamics

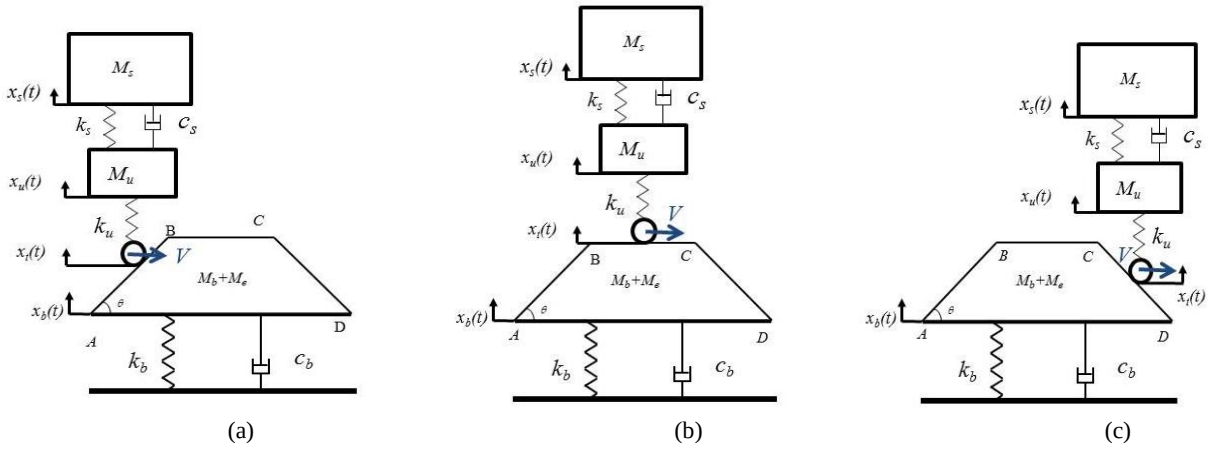


Figure 4-7. Interaction between SBEH model and vehicle model. (a) Vehicle is climbing on SBEH. (b) Vehicle is passing on top of SBEH. (c) Vehicle is going down the SBEH

In the combined modelling of vehicle and speed bump energy harvester, there are few things which are important to notice. Unlike the conventional input to the vehicle, the ground excitation, which is $x_i$ in this case, is fixed and doesn't depend on time. But, in this case, since the

speed bump is linearly movable, the input to the vehicle is both profile based and time dependent. We can compare this problem with the moving boundary condition where the boundaries are time dependent variable. Hence, another state along is introduced in order to take care of this problem.

Although, both the systems have their individual dynamics, when they come in contact they behave as a three- of four-body mass system (depending on the engagement or disengagement of the generator). Hence, the overall system can be represented in terms of three equations of decoupled masses when they come in contact. Governing equations of the overall system can be written as

$$M_s\ddot{x}_s + C_s(\dot{x}_s - \dot{x}_u) + K_s(x_s - x_u) = 0 \tag{28}$$

$$M_u\ddot{x}_u - C_s(\dot{x}_s - \dot{x}_u) - K_s(x_s - x_u) + K_u(x_u - x_t) = 0 \tag{29}$$

$$(M_b + M_e)\ddot{x}_b - C_b\dot{x}_b - K_b x_b - K_u(x_s - x_t) = F_p - F_g \tag{30}$$

Now, another point of consideration is, the stroke is limited to 2 inches in the prototype. Hence, as soon as the speed bump reaches its bottom most limit, the speed bump stops moving and the input to the quarter car is totally profile based rather than time dependent moving.

4.3.1.1 Input to the quarter car model

Section I: Tire position is located between A and B as illustrated in Figure 6 (a). The vertical velocity of the tire can be synthesized in terms of horizontal velocity of the vehicle tire *V*, which is taken as constant, and speed bump vertical velocity $\dot{x}_b$

$$\dot{x}_t = V\tan(\theta) - \dot{x}_b \tag{31}$$

Here, $\theta$ is the angle between the slope of the cover and ground.

Section II: Tire position is located between B and C as illustrated in Figure 6 (b). When vehicle tires reach point B on the speed bump, the profile input becomes zero as $\theta = 0$. Thus, the tire velocity in vertical direction becomes,

$$\dot{x}_t = -\dot{x}_b \tag{32}$$

Section III: Tire position is located between C and D as illustrated in Figure 6 (c). When vehicle tires cross the point C on the profile of the speed bump, the tire contact points begins to go down the slope of the speed bump. In that case $\theta$ will be negative and Eq. (13) will change to

$$\dot{x}_t = -V \cdot \tan(\theta) - \dot{x}_b \tag{33}$$

Figure illustrates the stages of input

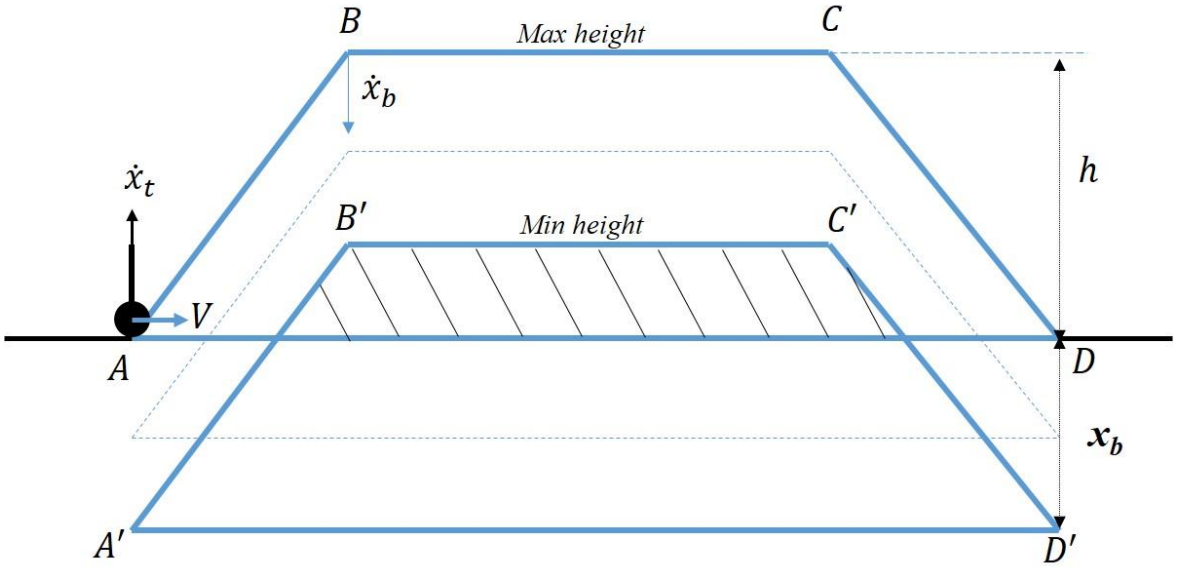


Figure 4-8 Different stages of the speed bump cover and inputs

Table 4-2 summarizes the different conditions for different inputs to the tire of the vehicle.

Table 4-2 Conditions for different inputs

| **Input/ Condition** | **If** $x_b < x_{b\max}$ | **If** $x_b = x_{b\max}$ |
|---|---|---|
| Between A & B | $\dot{x}_t = V\tan(\theta) - \dot{x}_b$ | $\dot{x}_t = V\tan(\theta)$ |
| Between B & C | $\dot{x}_t = -\dot{x}_b$ | $\dot{x}_t = 0$ |
| Between C & D | $\dot{x}_t = -V\tan(\theta) - \dot{x}_b$ | $\dot{x}_t = -V\tan(\theta)$ |

When the two-mass vehicle model is made to interact with SBEH model, the vehicle weight of $F_g = Mg$ exerted on the speed bump cover vertically downwards. Here, $M$ is the vehicle's overall

mass and *g* the gravity acceleration. Such a three-mass vibration system can be simplified and derived by synthesizing the SBEH model with the quarter vehicle but since the entire front axle will roll on the speed bump, we can double quarter vehicle model parameters i.e. double the sprung and un-sprung mass, double the suspension and tire stiffness and damping. Considering the three working stages of SBEH, the interaction between SBEH and vehicle can be analyzed as the following three stages.

(1) Before the speed bump cover reaches the bottom limit: During this process, the movement of the speed bump cover drives the rack via connecting rod which in turn rotates the pinions. During this phase, the rotational speed of the coupling shaft will be slower than the speed of pinion therefore the one-way clutch will engaged as described in earlier section

$$(M_b + M_{eq})\ddot{x}_b + C_{eq}\dot{x}_b + K_b x_b - K_u(x_u - x_t) = F_p - F_g \tag{34}$$

At the same time, vehicle works in a two-mass system as described by Eq. (22-23).

(2) After the speed bump reaches the bottom limit: When the speed bump cover reaches its hard stop or bottom most point, speed bump cannot move further and becomes stationary. At this moment, there is a complete state of disengagement and the dynamic equation of speed bump is switched and under the influence of static vehicle load, $F_g$ following equation will command the system

$$M_b\ddot{x}_b + K_b x_{b\max} = F_p - F_g \tag{35}$$

At the same time, the movable displacement boundary input to vehicle model will not change because $x_b = x_{bmax}$, and the profile of speed bump cover will act as profile input to vehicle as the conventional speed bump. $x_t$ will be the speed bump profile input to the vehicle model, which is the same as the tire rolling on the traditional speed bump with fixed boundary displacement input of speed bump profile. At this time, the speed bump energy harvester module and vehicle system has no interaction. Again, as in described in section 3.1, if $\dot{x}_b / R < \omega$, that is, the generator speed is higher than the rotational speed of pinion, one-way clutches are disengaged, and the speed bump energy harvester is separated from the speed bump cover unit. That is, the

equivalent mass and damping of harvester need not to be attached to attach to the model of speed bump cover. The one-mass vibration system of speed bump with the preload, can be expressed as,

$$M_b\ddot{x}_b + K_b x_{b\max} = F_p - F_g \tag{36}$$

Where, $x_{b\max}$ ,is the maximum stroke of the speed bump cover. Thus, $K_b x_{b\max}$ will always be constant. And the dynamics equation of energy harvester when both the one-way clutches are disengaged

$$M_e\ddot{x}_b + C_b\dot{x}_b = 0 \tag{37}$$

(3) Rebounding process when vehicle tires roll out of the speed bump cover: Since the vehicle weight is much large than the supporting force provided by the four springs of SBEH, the rebounding process only occurs when the vehicle tire move out of the speed bump cover when there is no interaction between speed bump and vehicle. Hence, as described in section 4.1, dynamic equation under the influence of static mass of the vehicle can be expressed as,

$$(M_b + M_{eq})\ddot{x}_b + C_{eq}\dot{x}_b + K_b x_b = F_p - F_g \tag{38}$$

To compare the influence of energy harvester with MMR to the dynamics of the interaction between speed bump and vehicle, a SBEH model where the rack and pinion is simple connected with the traditional electromagnetic generator without the MMR mechanism. Equations of the quarter car model will remain the same. However, the speed bump model in the three mass-spring vibration system can be described as the followings.

(1) Before the speed bump cover reaching the limiter: The dynamic equation of speed bump is derived from Eq. (22),

$$(M_b + M_e)\ddot{x}_b + C_b\dot{x}_b + K_b x_b - K_u(x_u - x_t) = F_p - F_g \tag{39}$$

(2) After the speed bump reach its limiter: As $\dot{x}_b = 0$ , the dynamic equation of speed bump is switched to the following equation

$$M_b\ddot{x}_b + K_b x_{b\max} - K_u(x_u - x_t) = F_p - F_g \tag{40}$$

(3) Rebounding process when vehicle tire rolling out of the speed bump cover: After the vehicle tire move out of the speed bump cover, the dynamic equation of the speed bump can be expresses as,

$$(M_b + M_b)\ddot{x}_b + C_b\dot{x}_b + K_b x_{b\max} = F_p \tag{41}$$

There is one point to be noticed, that the engagement and disengagement are individual phenomenon which depends on the state of the system and moreover, vehicle parameters. Here, energy harvester can go from engaged to disengage state, or vice-versa, at any point when the vehicle is on the speed bump cover. Hence, the engagement and disengagement should be confused with the stage the vehicle is on. The following table summarizes the relationship between stage and the state of the system.

Disengaged status:

$$(\dot{\theta}_{pj} - \dot{\theta}_b) < 0\,, T_c = 0 \tag{42}$$

$$M_{eq}\ddot{x}_b + C_{eq}\dot{x}_b = 0 \tag{43}$$

Engaged status:

$$(\dot{\theta}_{p1} - \dot{\theta}_b) \geq 0\,, T_c = K_{c1}(\theta_{p1} - \theta_b) \tag{44}$$

$$M_t\ddot{x}_b + C_{eq}\dot{x}_b = F \tag{45}$$

### 4.3.2 Speed bump modelling with half car dynamics

Speed Bump modelling with half car dynamics is similar to that of the combined quarter car and harvester modelling, except, here, we have more degrees of freedom from the vehicle's end. Following figure is the representation of the combined half car and speed bump energy harvester.

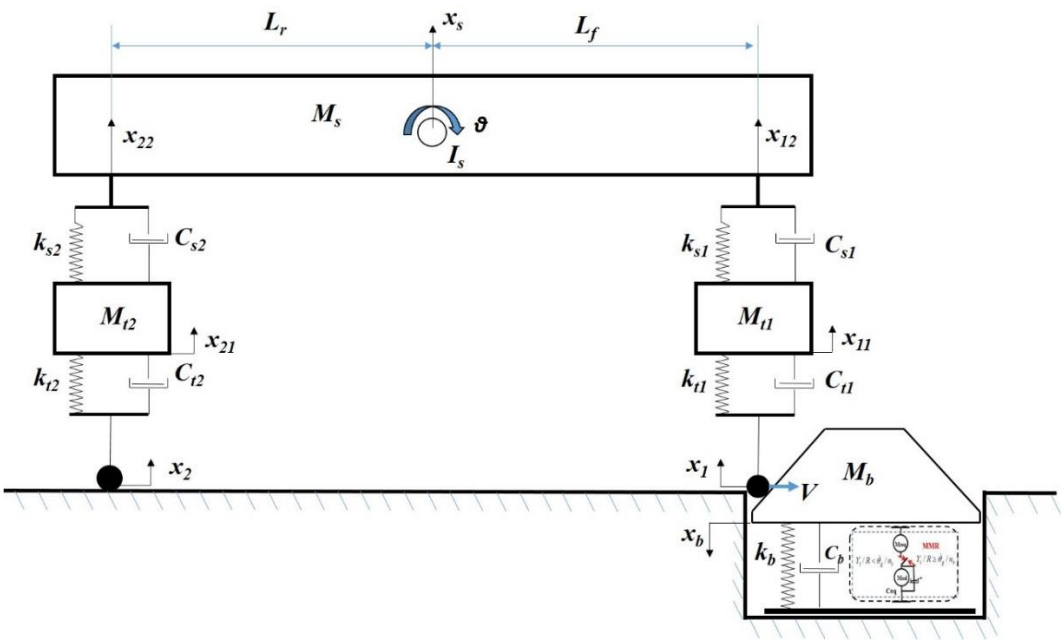


Figure 4-9 Combined model of the speed bump energy harvester and half car

## 4.4 Energy generation

The harvested power can be obtained from the multiple of torque and the generator rotation in Equation (1) and (2),

$$P = T_g \cdot \dot{\theta}_g = \frac{K_g K_t \cdot \dot{\theta}_g^{\,2}}{(R_i + R_0)} \tag{46}$$

According to the relationship of the generator rotation speed with the speed bump up-down movement, $\dot{\theta}_g = \frac{n_b \dot{x}_b}{r}$, the harvested power can be expressed as,

$$P = \frac{K_g K_t \cdot n_b^2 \dot{x}_b^{\,2}}{(r^2 (R_i + R_0))} \tag{47}$$

According to the equivalent mass and damping in Eq. (17), Eq. (47) can be simplified as

$$\boldsymbol{P = C_{eq} \dot{x}_b^{\,2}} \tag{48}$$

The velocity $\dot{x}_b$ can be calculated according by solving all the equations of motion numerically either by Ranga-Kutte or Euler's method.

# 5 Experiment

## 5.1 Lab test

Dynamic performances of the fabricated prototype are measured by a dynamic measurement system in lab as shown in Figure 5-1. In order to evaluate the dynamic response of the harvester to vibration excitation, multiple-channel measurement system is set up. Laser displacement sensor is used to measure movement of speed bump cover. Accelerometer measures acceleration of the vibration speed bump cover. The harvested electricity can be measured by a circuit for three phase voltage as shown in Figure 5-2 (right). The test is to measure the electrical power output and performance of speed bump energy harvester by jumping on speed bump cover.

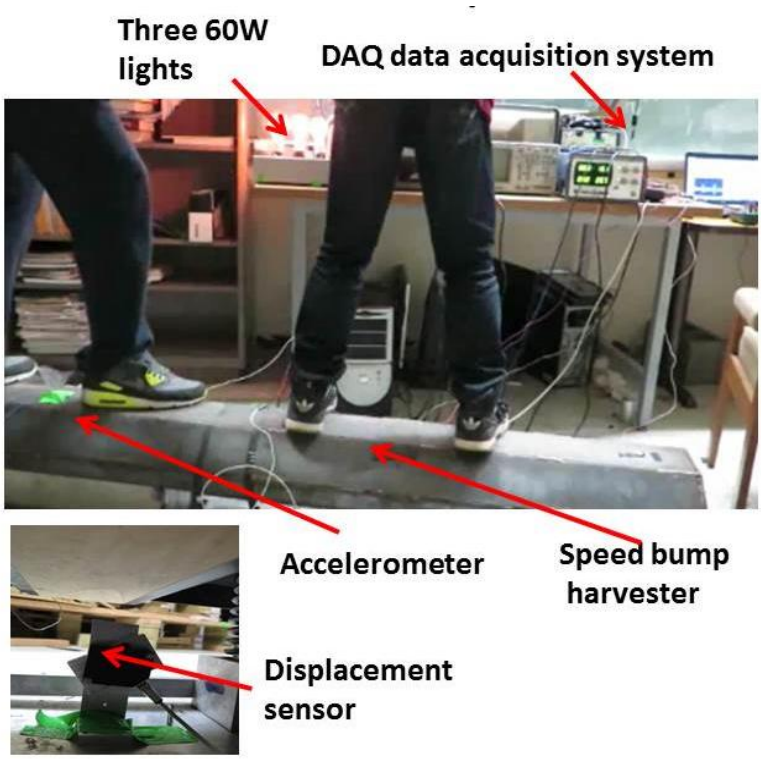


Figure 5-1 lab testing of the speed bump energy harvester connected with the data acquisition system and displacement and acceleration sensor

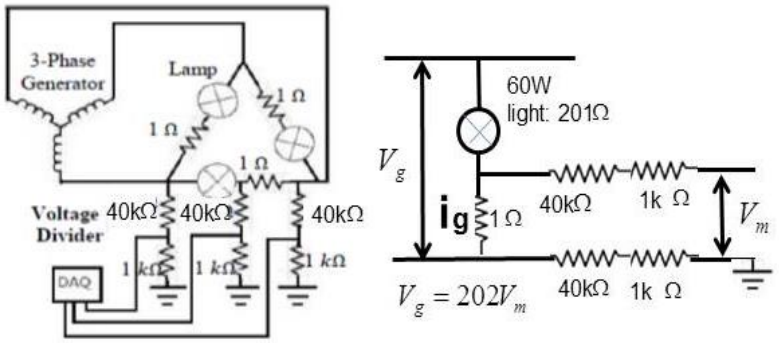


Figure 5-2 (left) - electrical circuit for the brushless DC motor/generator (right) - resistance circuit for the BLDC motor/generator

## 5.2 In-field test

In-field test is carried out by setting up a wooden ramp almost 2 ft high. The reason for setting up a ramp is because, it was virtually impossible to get permission to dig a rectangular hole where the speed bump energy harvester could be placed. Instead, the idea of elevating a ramp like structure is brought in and the speed bump is placed between two ramps so that a car could easily run over it and the prototype could be tested. The setup of the in-field testing is shown in Figure 5-4. The advantage is this platform can be easily assembled for the test without breaking the concrete surface and digging a hole on the road and can be easily disassembled after the test.

Multiple-channel measurement system is built up to evaluate energy harvesting capability, the vibration of both speed bump energy harvester and vehicle. Accelerometers are mounted on both speed bump cover and vehicle body and unspring mass (tire) to evaluate shock responses. And laser displacement sensor is mounted on speed bump cover to measure the impulse input and displacement. The harvested electrical voltage and current can be measured by a circuit for three phase voltages with three 60W lights in Y shape, as shown in Figure 5-1 (left). The electrical lights and the measurement resistors of 1 Ohm are the external resistance. A passage car of Honda Civic is used as the test vehicle.

Figure 5-3 Preliminary in-field testing. Car being driven on the elevated ramp getting in contact with the speed bump energy harvester

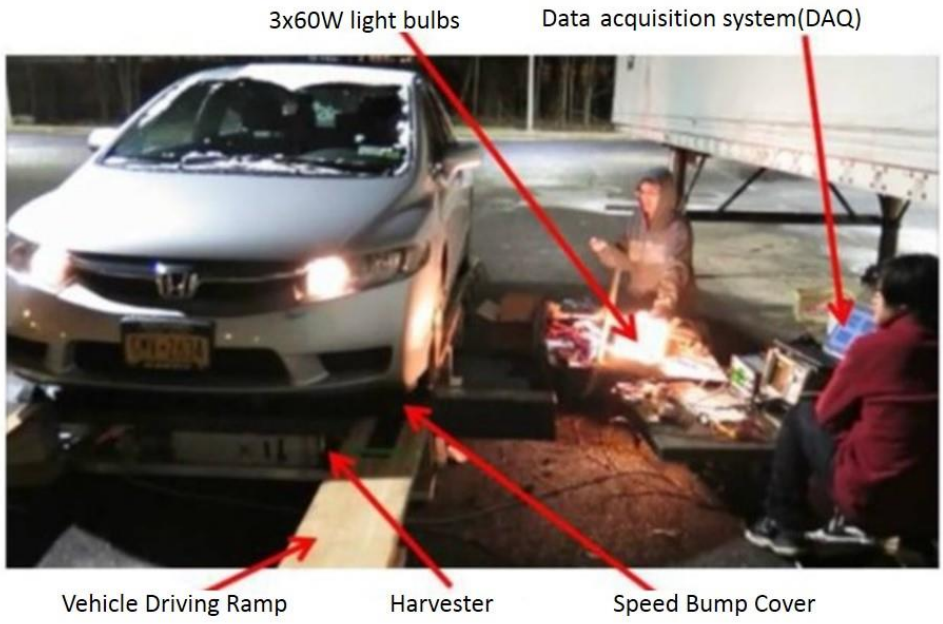


Figure 5-4 final in-field testing of the speed bump energy harvester.

## 5.3 Limitations of in-field tests

There were several limitation of which, these are the major limitations that were faced during the in-field testing of the prototype:

1. The elevated ramp was small in width hence making it really hard for the driver to keep the vehicle aligned or straight over the ramp.
2. Since, there was always a chance of car being fallen from the elevated ramp, there was a serious limitation on the velocity with which the driver could drive on the ramp. This limited the testing velocity to only 2 MPH.
3. Since there was a velocity limitation, thorough in-field testing was barred and results are limited to support the simulation results which are discussed in the later sections.
4. Vertical body acceleration of the vehicle could not obtained, thus, research is extensively relied on simulation study. Although, there is enough data to claim the hypothesis presented in chapter 2.

# 6 Results and discussion

## 6.1 MMR: Its effectiveness and effects on quarter car dynamics

The initial study of the combined quarter car and speed bump energy harvester is conducted to validate the effectiveness of MMR and to know whether is there any effects on the quarter car model by its usage. For this, the quarter car model of the vehicle is used from the literature. The parameters for the quarter car model are given in the Table 6-1

Table 6-1 Detailed parameters for the quarter car model

| **Parameters** | **Notation** | **Value** | **Unit** |
|---|---|---|---|
| Radius of Pinion Gear | $R$ | 0.0254 | $m$ |
| Sprung Mass | $M_s$ | 1527 | $kg$ |
| Un-Sprung Mass | $M_u$ | 200 | $kg$ |
| Speed Bump Mass | $M_b$ | 150 | $kg$ |
| Equivalent mass | $M_e$ | 620 | $kg$ |
| Total Mass (Speed bump and equivalent mass) | $(M_b+M_e)$ | 770 | $kg$ |
| Suspension Stiffness | $K_s$ | 60000 | $N/m$ |
| Tire stiffness | $K_s$ | 440000 | $N/m$ |
| Speed bump stiffness | $K_b$ | 130000 | $N/m$ |
| Suspension damping coefficient | $C_s$ | 7000 | $N\text{-}s/m$ |
| SBEH electrical damping coefficient | $C_e$ | 400 | $N\text{-}s/m$ |
| Gravitational constant | $g$ | 9.8 | $m/s^2$ |
| Gear Ratio | $n$ | 50 to 1 | |

### 6.1.1 Effectiveness of MMR

As claimed earlier, MMR increases the overall density of the power generated, hence, increasing the average power output. Figure 6-1 illustrates the dynamics pinion gear and the generator shaft and the functioning of the MMR.

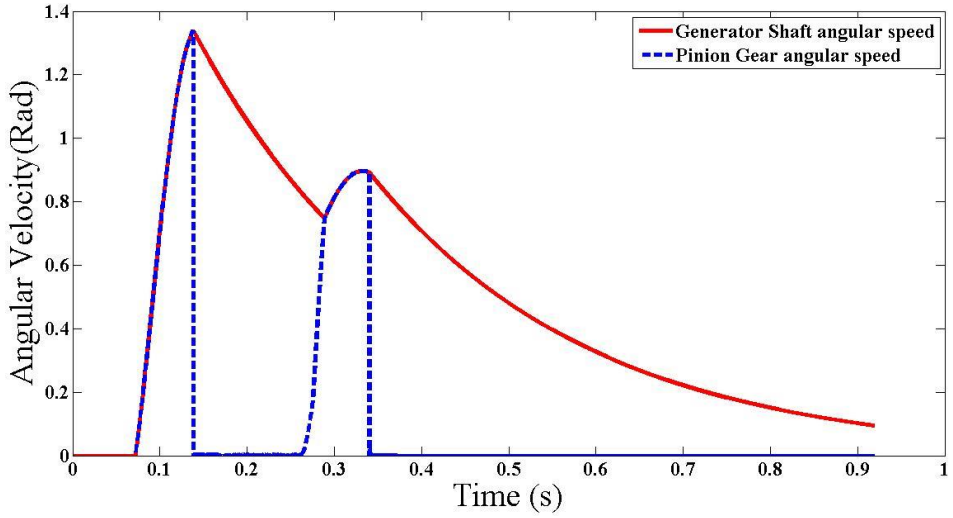


(a)

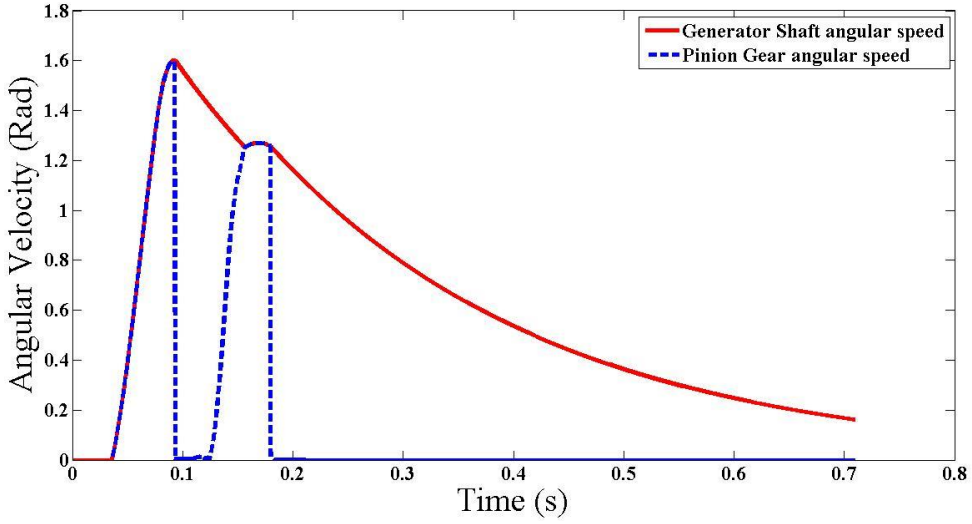


(b)

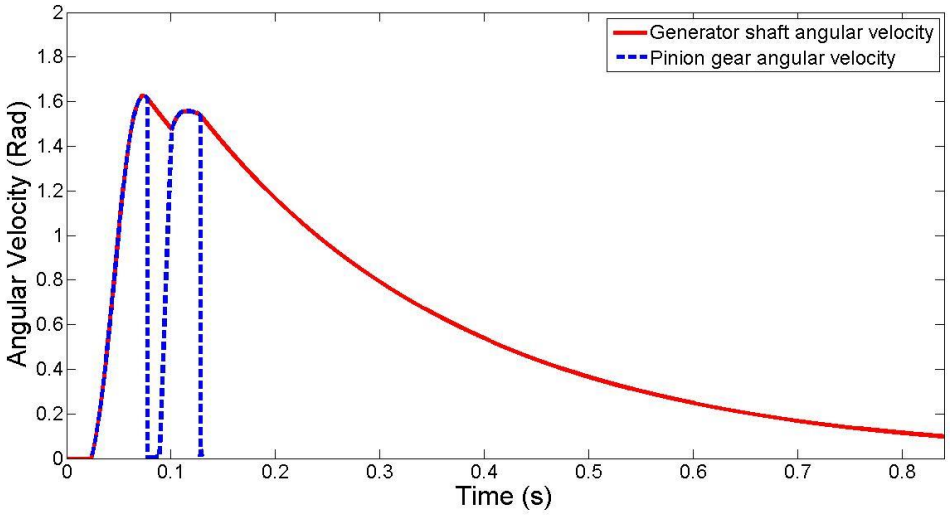


(c)

Figure 6-1 comparison of pinion gear angular velocity and generator shaft angular velocity at (a) 2 MPH (b) 5 MPH and (c) 10 MPA

Figure 6-1 represents the behavior of the angular velocities of the pinion gear and generator shaft at 2, 5, and 10 MPH vehicle speed. The engagement and disengagement phenomenon of the MMR is clearly seen in these three graphs. The dark line represents the angular velocity of the generator shaft, whereas, the dashed line represents the angular velocity of the pinion gear. As the vehicle starts running over the speed bump, the speed bump cover moves down and drives the rack and pinion assembly. Hence, the system is engages pinion gear drives the generator shaft with the same angular velocity. As soon as the rack reaches its bottom limit, the pinion stops and its angular velocity suddenly falls to zero. Thereafter, the system disengages and the generator shaft keeps rotating with a decay factor of

$$\dot{\theta}_g = \dot{\theta}_g e^{-\left(\frac{C_{eq}}{M_{eq}}\right)*t} \tag{49}$$

The same trend is followed by the power generated since it is directly proportional to the square of angular velocity of the generator shaft. The second peak seen in the figures indicated the engagement of the system during the rebounding process.

Another point to notice here is, as the velocity of the vehicle increases, the peaks come closure together. This make sense because, at higher speeds, the time tire remains on the speed bump get lower and lower. Hence peak coming closure is the validation of it.

### 6.1.2 Effect of MMR on quarter car vehicle dynamics

It is important to know if the MMR plays any role in changing the dynamics of the quarter car model. This simulation is used to validate the dynamic effect of speed bump energy harvester on the vehicle dynamics. Figure 6-2 is the comparison of the dynamics of coupled quarter car and speed bump energy harvester with and without MMR.

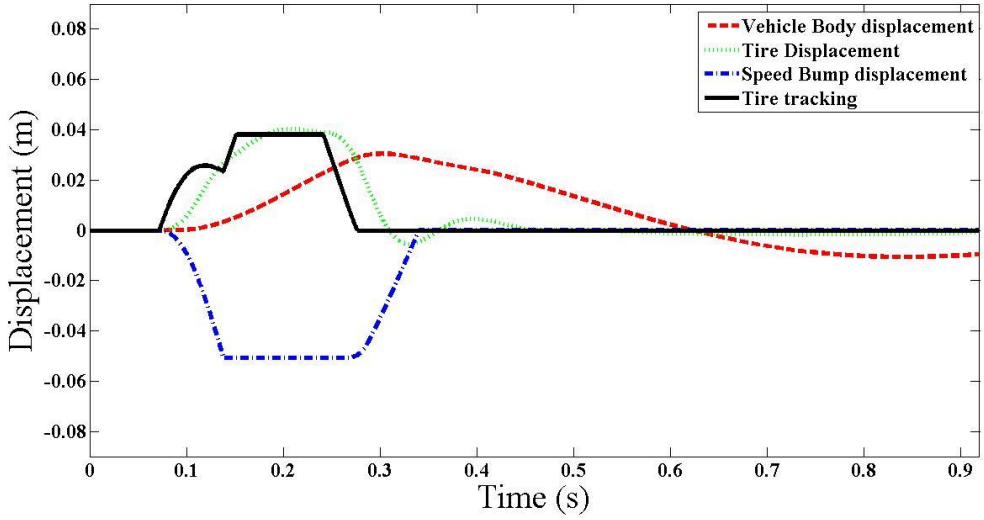


(a)

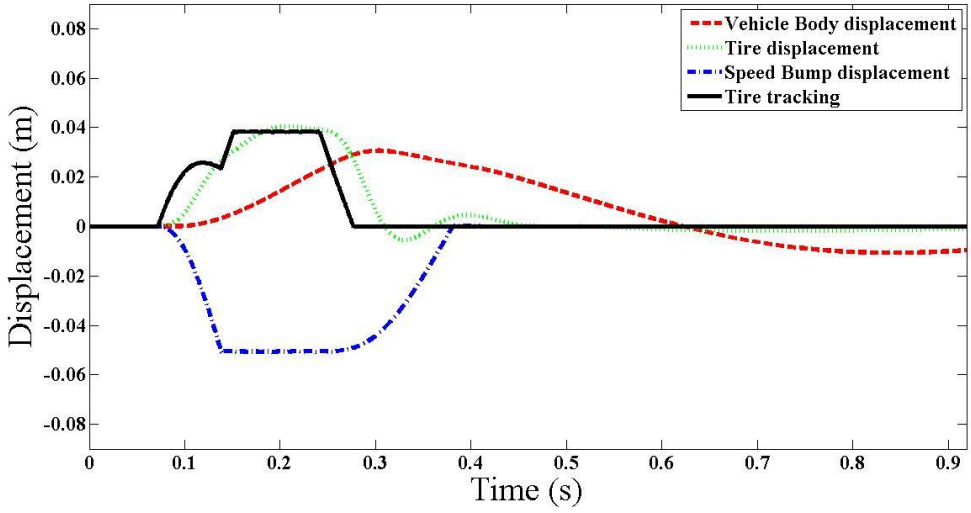


(b)

Figure 6-2 simulation results for the speed bump displacement, sprung and un-sprung mass of the quarter car model at 2 MPH with (a) MMR (b) Non-MMR

In above Figure 6-2, tire tracking is the point of contact between the tire and the speed bump cover. A dip in the tire tracking point indicates that, first, the tire starts to running over the speed bum cover and gains some height. After some time, due to the effect of vehicle dynamics, the speed bump starts to gain the stroke and hence, moves down. At the same time, the tire also takes a dip and hence, the tracking line drop until the speed bump cover reaches its bottom most limit. Thereafter, the speed bump cover behaves like a conventional speed bump. This validates the modelling of the system. From Figure 6-2 it can be seen that the displacement of the vehicle body, tire and the speed bump hardly changes. That means, MMR doesn't really affect the dynamics of the vehicle. Only the dynamics of the speed bump changes which is not a concern for the rider riding the vehicle.

### 6.1.3 Comparison of power generation

Figure 6-3 shows the power generated by the MMR enabled harvester and non-MMR case. A non MMR case can be attributed to a simple linear generator which doesn't have the capability to rectify the angular motion of the shaft and hence, as soon as the speed bump reaches the bottom limit, the shaft, along with the pinion and rack assembly, stops moving and generator generates no power until, the vehicle completely passes over the bump cover and the rebounding process starts again. In Figure 6-3, there are two peaks which highlight two way motion of the harvester. First peak is because of the down stroke, and the second peak of the power is up stroke or rebounding of the bump cover. As we can note, the area under the curve is larger in case of MMR enabled harvester at both the speeds. By integrating the curve in both the cases, the area under the curve, or energy, is at least 3-4 times higher in case of MMR enabled system. Hence, MMR has a due advantage over the conventional non MMR/Linear generator type harvester which is claimed in the previous research[78].

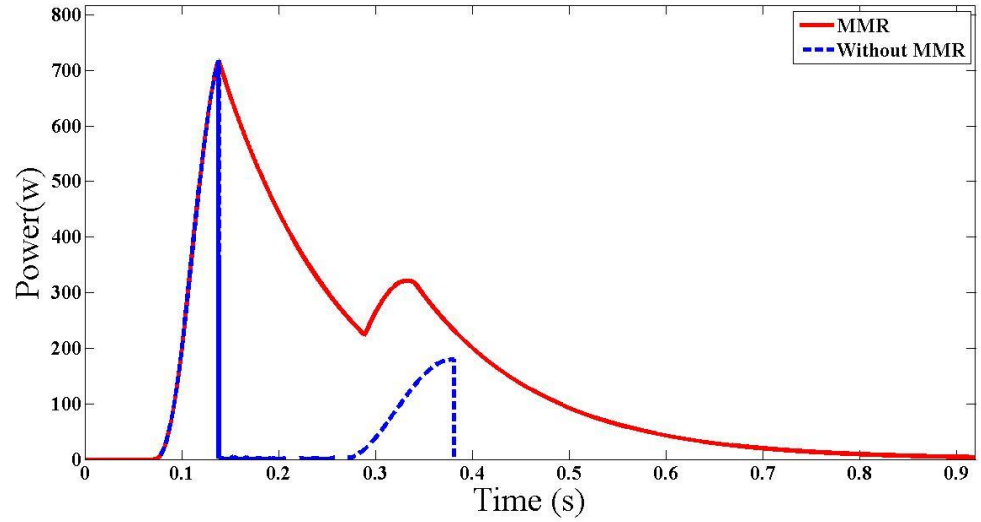


(a)

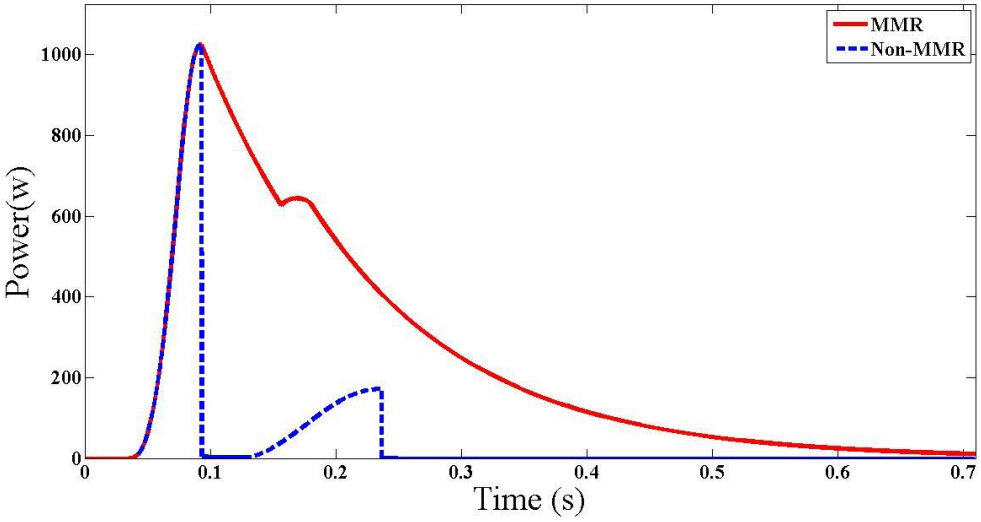


(b)

Figure 6-3 power generation in MMR and Non-MMR case at (a) 2 MPH (b) 5 MPH

Similarly, at 5 MPH, the result is the same results are occupied. Figure 6-4 indicates the dynamics and the energy harvested at 5 MPH.

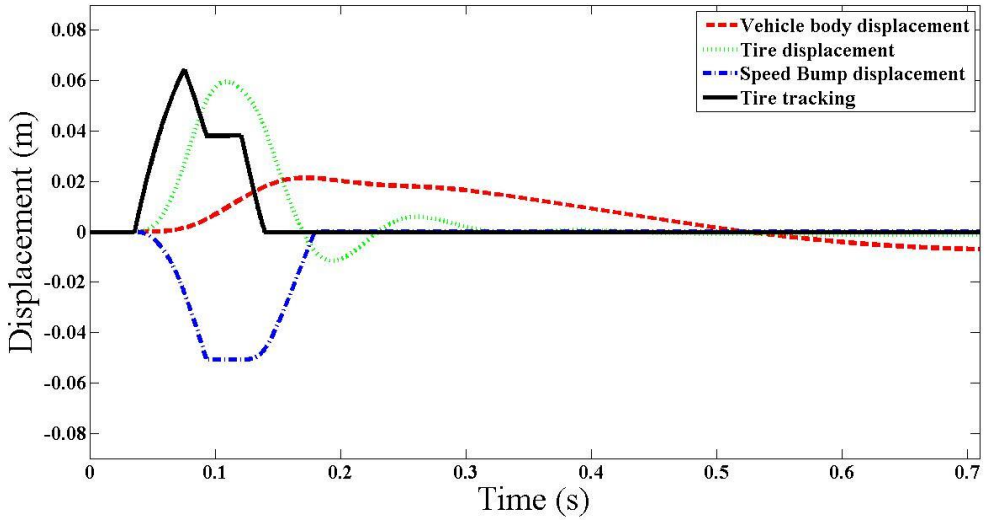


(a)

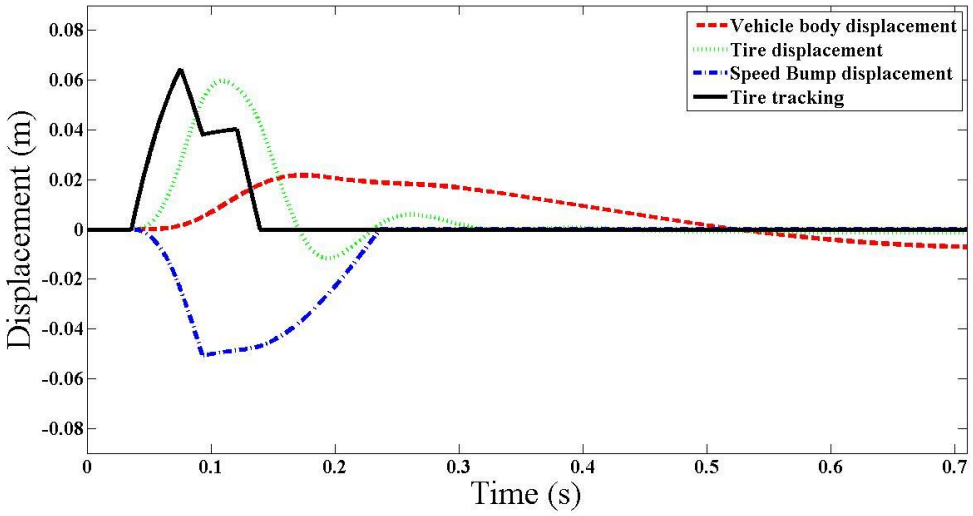


(b)

Figure 6-4 simulation results for the speed bump displacement, sprung and un-sprung mass of the quarter car model at 5 MPH with (a) MMR (b) Non-MMR

Now, as the effectiveness of MMR in the energy harvesting is confirmed, the effects of speed bump energy harvester is studied extensively in the following section 6.2. For this, the half car vehicle model has been selected for the study as illustrated in the Figure 4-9 in chapter 4.

## 6.2 Effects of energy harvester on half car vehicle dynamics

As it is ascertained by simulation in the previous section that MMR has a huge advantage of generating more power as compared to a non-MMR or linear generator case, it will be intriguing to simulate the system close to real scenario. For this purpose, the half car model is used for the study and the impact of speed bump energy harvester is studies in more depth in this section. The overall system is represented in the Figure 4-9 in chapter 4. The parameters of different vehicles types have been taken from the literature [39]. Speed bump parameters remain the same.

Table 6-2 Parameters for half car model of class D (Mid-size sedan)

| **Parameters** | **Notation** | **Value** | **Unit** |
|---|---|---|---|
| Sprung mass | $M_s$ | 1527 | *kg* |
| Front tire mass | $M_{t1}$ | 100 | *kg* |
| Rear tire mass | $M_{t2}$ | 80 | *kg* |
| Front suspension Stiffness | $K_{s1}$ | 30000 | *N/m* |
| Rear suspension Stiffness | $K_{s2}$ | 30000 | *N/m* |
| Front tire stiffness | $K_{t1}$ | 220000 | *N/m* |
| Rear tire stiffness | $K_{t2}$ | 220000 | |
| Front suspension damping coefficient | $C_{s1}$ | 3500 | *N-s/m* |
| Rear suspension damping coefficient | $C_{s2}$ | 3500 | *N-s/m* |
| Front tire damping coefficient | $C_{t1}$ | 0 | *N-s/m* |
| Front tire damping coefficient | $C_{t2}$ | 0 | *N-s/m* |
| Gravitational constant | $g$ | 9.8 | $m/s^2$ |
| Gear Ratio | $n$ | 50 to 1 | |

### 6.2.1 Tire deflection

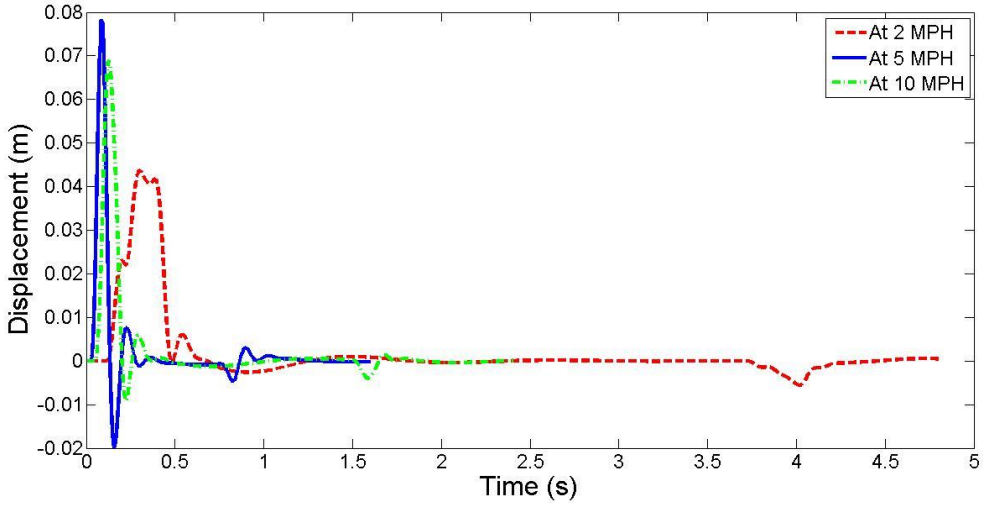


(a)

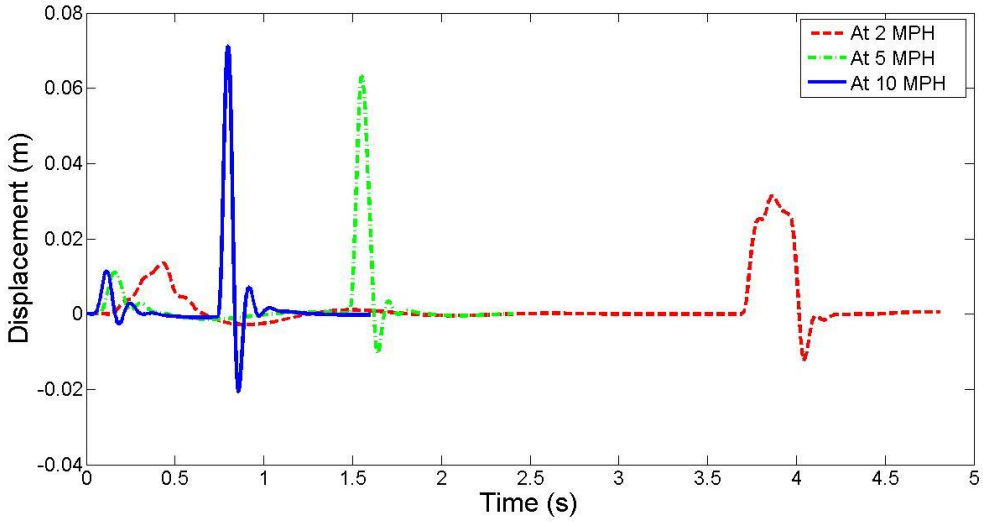


(b)

Figure 6-5 Tire deflection at optimal speed of 7 MPH for (a) front tire, (b) rear tire

Figure 6-5 show the front and the rear tire deflection of the vehicle. As it is seen here that as the velocity increases, front and the rear tire deflection drops from 0.07 in to a range of 0.03 in. This occurring in the tires indicate that lesser deflection will be transferred to the sprung mass of the half car model. It is validated in the following sections of body bouncing and pitching

### 6.2.2 Tire deformation

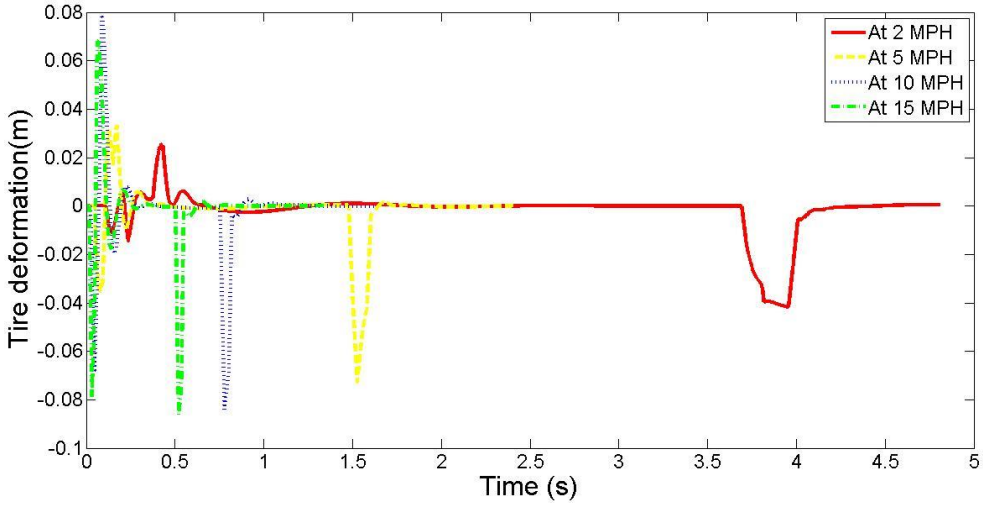


(a)

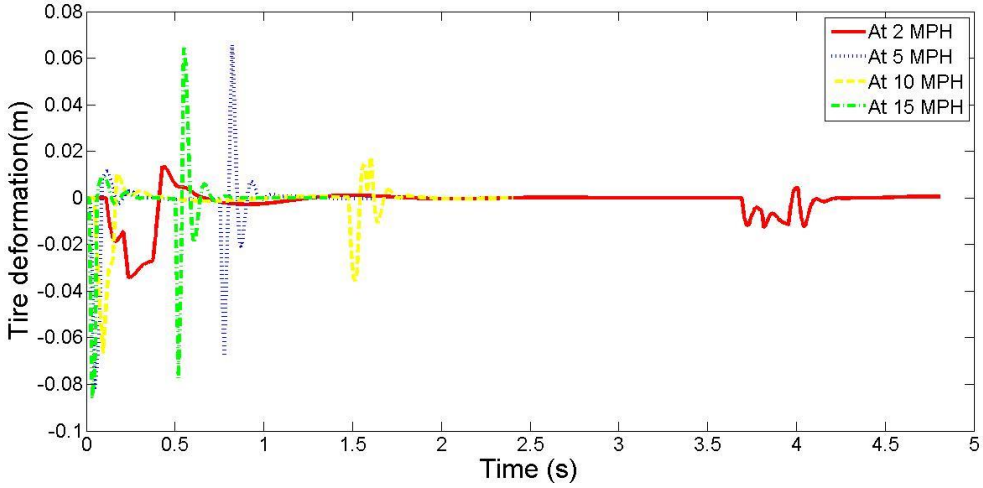


(b)

Figure 6-6 tire deformation of the vehicle at optimal vehicle speed of 7 MPH of (a) front tire, (b) rear tire

Comparisons of the front and the rear tire deformation is shown in Figure 6-6. Trend shows that at higher velocities, the tire tends to absorb more compression due to speed bump profile shape. It significantly increase from the mark of 0.02 in, at a speed of 2 MPH, to around 0.075 in at 15 MPH.

### 6.2.3 Front and Back body deflection

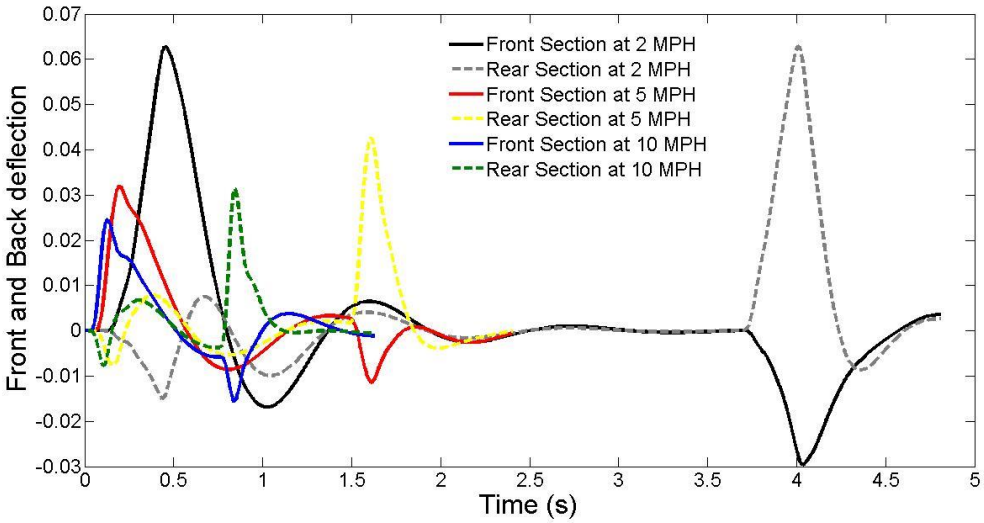


Figure 6-7 Front and back body deflection magnitude

In figure 6-7, the dashed lines represents the rear portion of the vehicle and the solid lines represents the front portion of the vehicle at various possible velocities. As the front portion, at all the given velocities, travel through the bump, gains the height and rear portion drops the height which makes sense. Trend shows that as the deflection magnitude is inversely proportional to vehicle velocity.

The major aim of this simulation is to check whether there is any anomaly in the results. It appears that, in the front and back body deflection, the maximum deflection occurs at the speed of 2 MPH. This behavior is assumed normal because at lower velocity there will be less energy absorption by the damper and since at the given velocity, vertical velocity is also pretty low as suggested in Equations (31)-(33).

### 6.2.4 Bouncing and Pitching

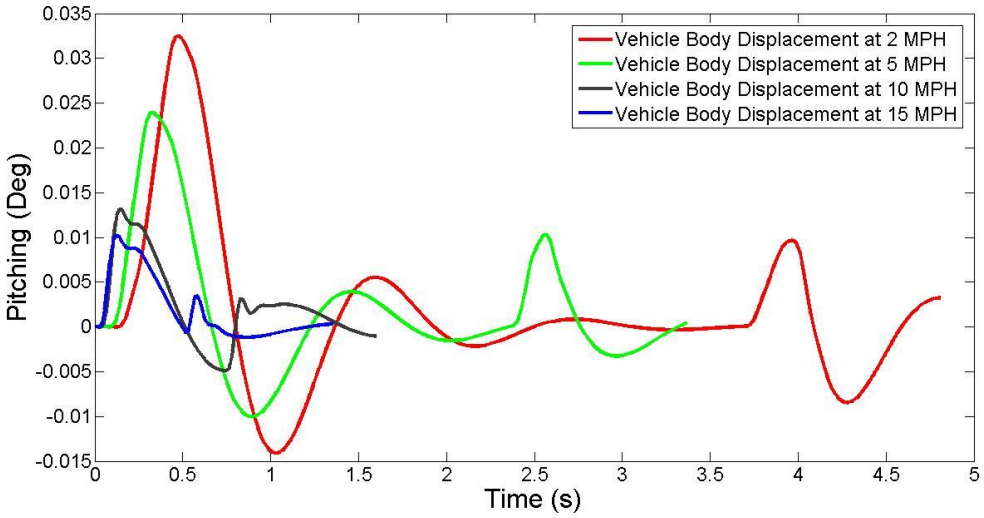


(a)

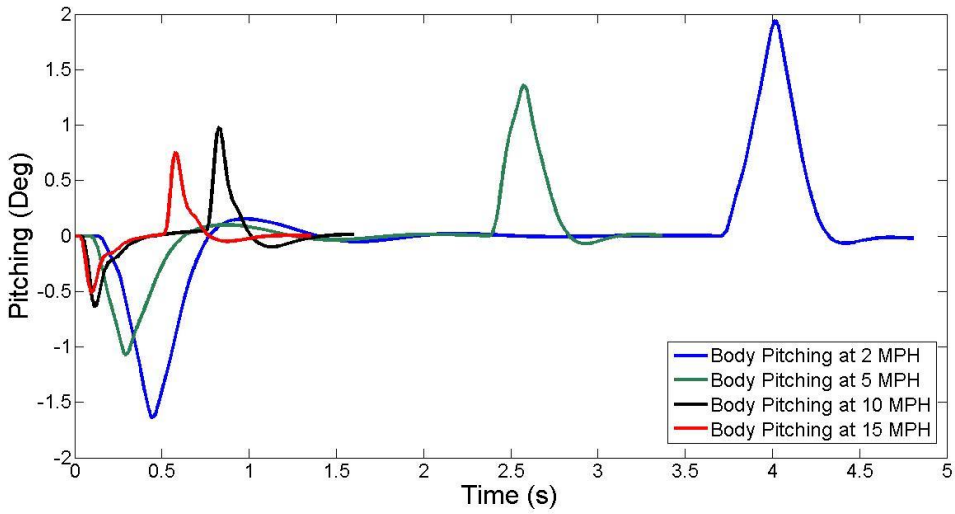


(b)

Figure 6-8 Vertical displacements of the sprung mass in half car model where (a) is the bouncing, and (b) pitching of the sprung mass

Figure 6-8 shows the bouncing and pitching behavior of the vehicle sprung mass. As expected, the bounding and pitching in the vehicle reduced as the vehicle velocity increases as most of the energy is absorbed by the vehicle dampers and not transferred to the sprung mass.

### 6.2.5 Body Acceleration

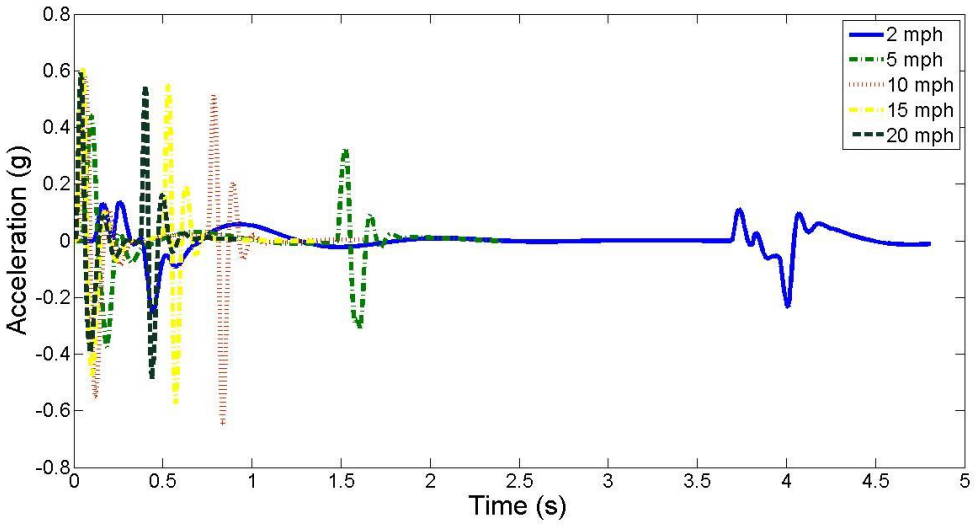


Figure 6-9 vertical sprung mass acceleration of class D vehicle at various velocities

Body acceleration is one of the main criteria to study the effects of speed bump energy harvester on the vehicle. Figure 6-9 shows the body acceleration of the sprung mass at different velocities. One of the advantages of the speed bump energy harvester, as claimed in the beginning, is that it uses the potential and kinetic energy of the vehicle to harvest energy. This means, that the shock that is supposed to be absorbed by the vehicle suspension is absorbed by the harvester instead. This results into decreased body vertical acceleration of the vehicle and thus, keeping rider in the comfort zone for a wide range of velocities.

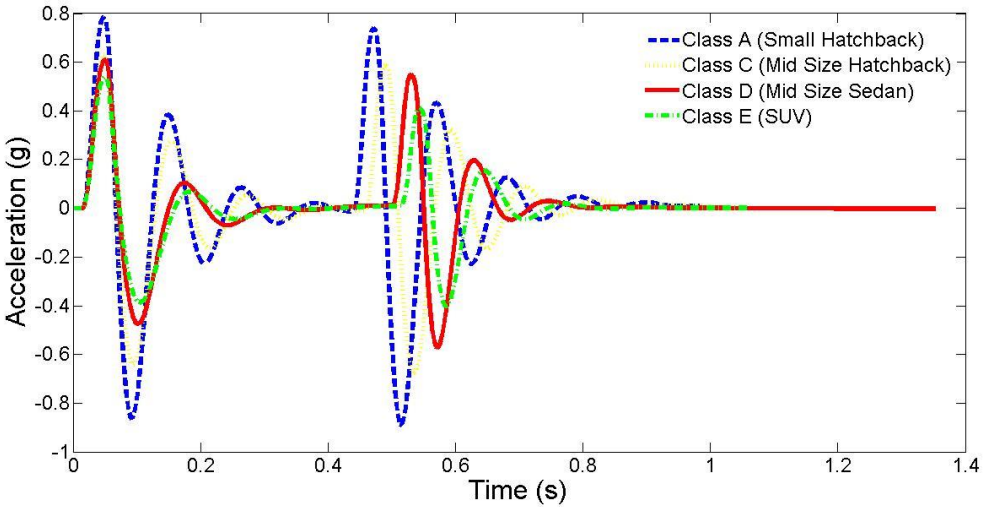


Figure 6-10 Vertical acceleration for all classes of vehicles at 15 MPH

In previous literature, it has been mentioned a lot of times, that speed bumps pose a threat to the rider driving the vehicle as it is, geometrically, more aggressive than the humps since they are short and provide an immediate vertical challenge to the vehicle causing a considerable damage to the vehicle and the rider if the vehicle is driven at a large speed[79] since it is mainly used to check the vehicle speed within 5 MPH. The main advantages of the speed bump energy harvester is supposed to take care of this issue by resolving the energy transfer from tires to the vehicle body. Instead, the energy that is supposed to be transferred to the vehicle body is absorbed by the harvester to produce more power. Figure 6-9 suggests and validates the hypothesis. It is seen that even at higher speed, as high as 20 MPH, the vertical acceleration of the vehicle sprung mass is within the 1g limit.

## 6.3 Effects of Vehicle parameters on energy generation

The study of the energy harvester on the vehicle dynamics has been done in the previous section 6.2. But it is important to understand the effect of different kinds of vehicles on the power generation of the energy harvester. For example, a vehicle with a gross weight of 3000 lbs will not have the same effect on the speed bump energy harvester as compared to vehicle with 5000 lbs. This assumption leads to the study of the dynamics of the harvester on changing the model of the vehicle.

For this simulation study, different classes of vehicles are taken into consideration from the literature [39]. Vehicle class A, C, D, E, and F are considered for the simulation. Class A is a small hatchback car, Class C is a mid-size sedan, Class D is full size sedan, class E is the SUV vehicle and F is the 6 wheeled truck. The parameters for Class A- E are taken from the literature[39].

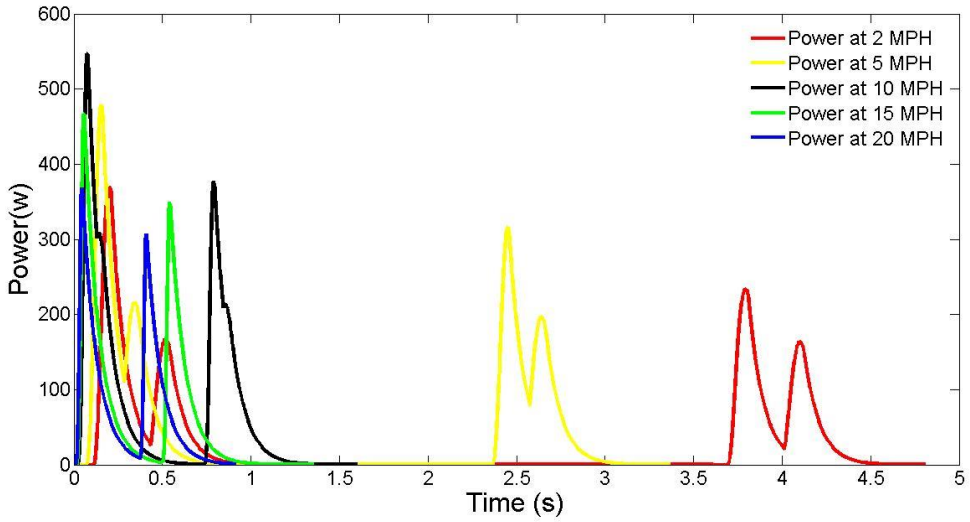


Figure 6-11 energy graph from class D vehicle at various possible velocities

The simulation study is performed on various classes of vehicles on different velocities on different

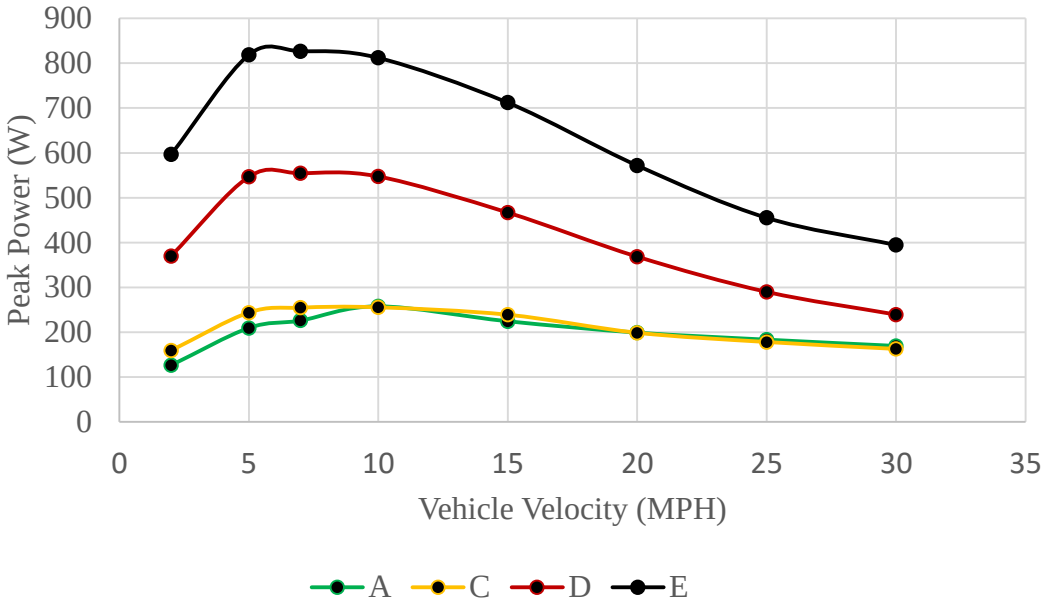


Figure 6-12 comparison of the peak power for various classes of vehicles at different velocities

In Figure 6-12, it is seen that for various class of vehicles, the harvested peak electrical power if different depending on the size of the vehicle. Hence, it can be said that the higher the weight of the vehicle, more peak power can be harvester out of harvester. It is important to know

the energy and the RMS power obtained by the harvester. Figure 6-13 (a) and (b) show the simulation result of the harvested electrical power in terms of total energy and RMS value.

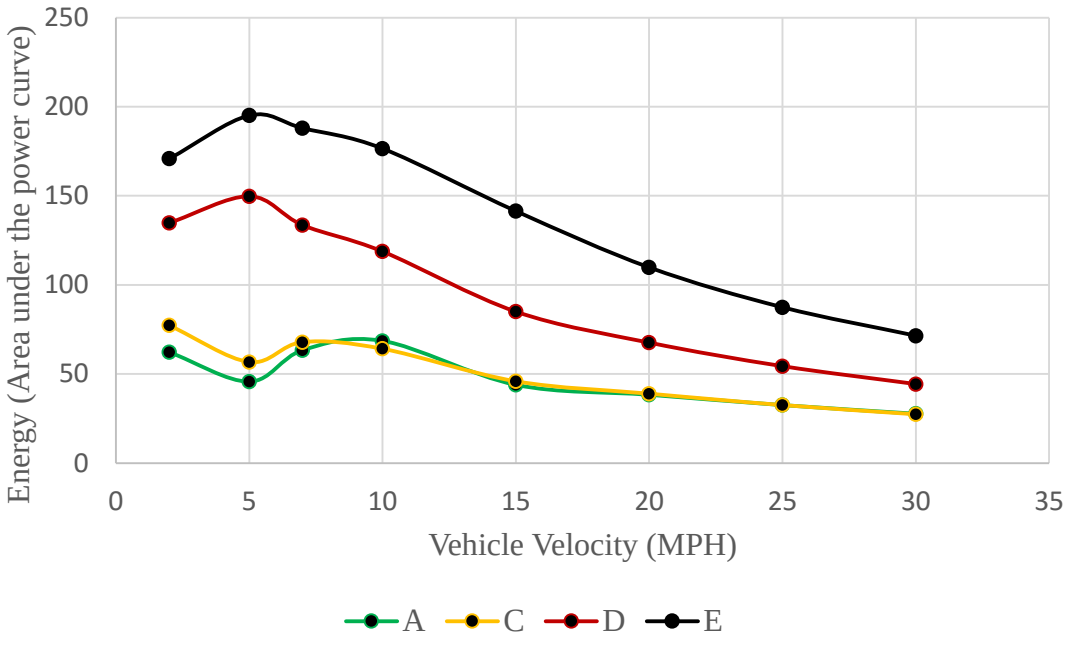


(a)

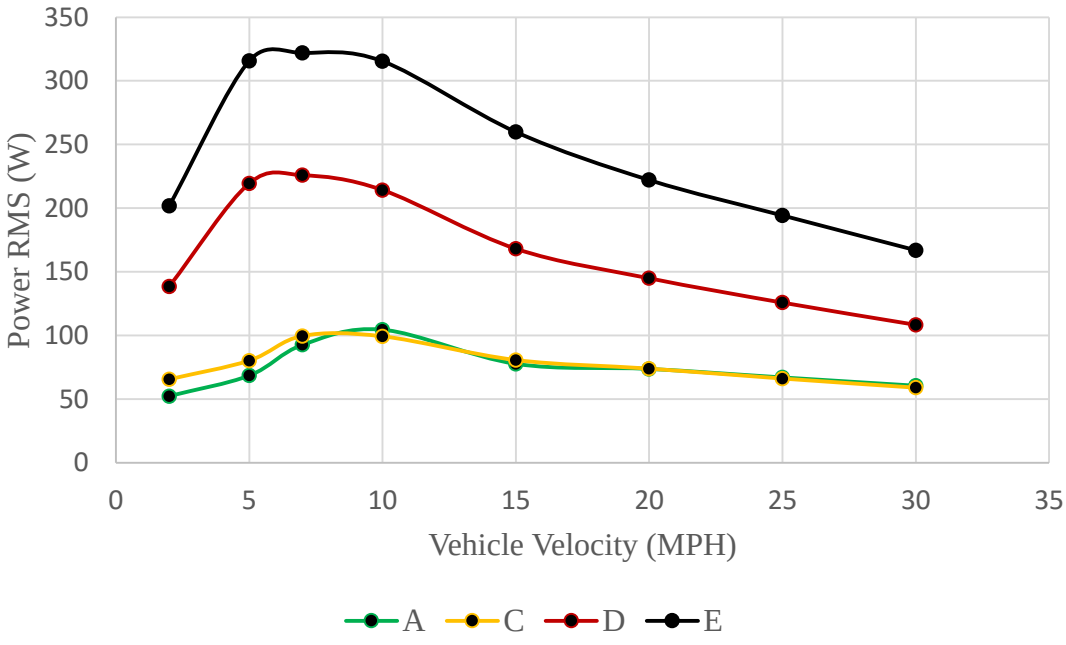


(b)

Figure 6-13 Total energy graph vs Vehicle velocity, (b)- RMS Power vs Vehicle velocity graph.

In the Figure 6-13 (b), the maximum RMS and peak power is obtained around 7 mph. It suggests that the maximum power which can be harvester comes at around the 7-10 mph vehicle velocity range from all classes of vehicles. Hence, it is important to see whether around this velocity, what is the influence of the external load i.e. external resistance since the expression of the power generated is given as in Equation (44). The study of the effects of external load is done in the next section.

## 6.4 Effects of external load on energy generation

It is known that the external load is indirectly proportional to the electrical damping as described in Eq. (44) in the previous section. Therefore, higher the external load, lesser will be the electrical damping and hence, power generation. In this section, the effects of external load on energy generation is studied with the help of simulation. For the simulation, the velocity of the vehicle is kept around 7 -10 mph which also should be the optimal velocity range for the power generation.

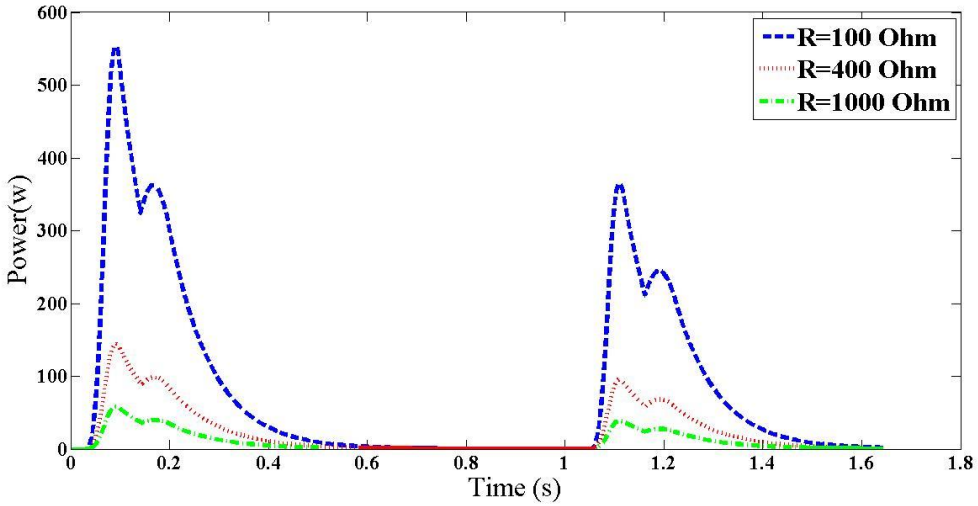


Figure 6-14 Electrical power at different external resistance.

## 6.5 Effects of the equivalent mass and flywheel on energy harvesting

The effects of a flywheel must have an effect on energy generation. Although, the prototype built for the testing doesn't include a flywheel, it would be important to know its effects on energy generation. For that purpose, a theoretical model of the equivalent mass in Equation (4) is added with a inertia of the flywheel. Therefore, Equation (4) would change to;

$$M_{eq} = \frac{(I_s + n^2(I_g + I_f))}{r^2} \tag{50}$$

Where, $I_f$ is the inertial mass of the flywheel, $r$ is the radius of the driving shaft, $I_g$ is the inertial of the generator rotor and $n$ is the gear ratio. Inertial mass, $I_f$, is calculated by

$$I_f = \frac{1}{2} M R_f^{\,2} \tag{51}$$

Where, $R_f$ is the radius, and $M$ is the mass of the flywheel. Class D, which is the most common vehicle on road, is used to study the effects of flywheel on the vehicle at 7 mph. This velocity is selected for this simulation study because around 7 mph, we get the maximum rms power. Hence it will be wise enough to see what would be the effect of the flywheel on the power generation.

Since, there is not enough space inside the enclosure of the harvester, it is not possible to increase the radius of the flywheel. Hence, to increase the overall mass of the flywheel, different thickness of flywheel equivalent to masses, 1.5 kg, 2 kg, 2.5 kg, and 3 kg are used in the simulation.

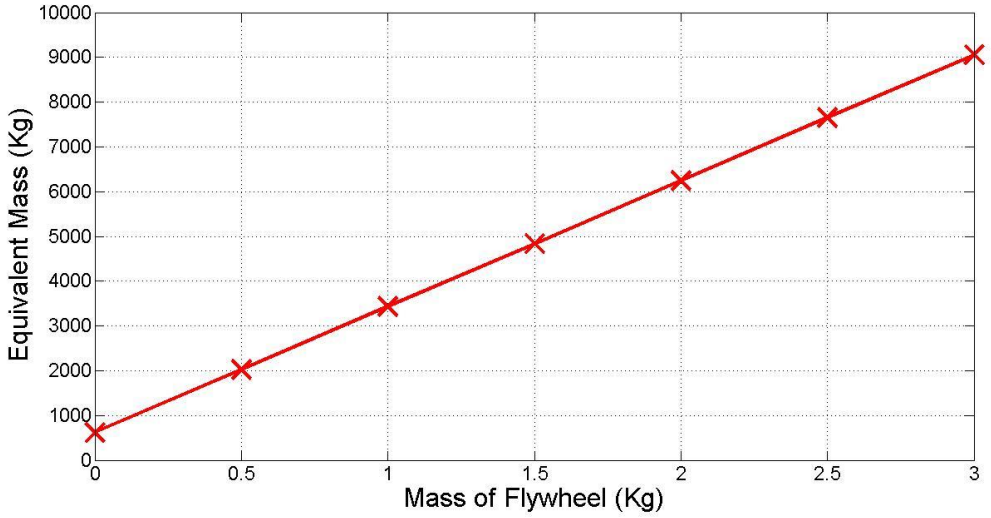


Figure 6-15 Change in equivalent mass by changing mass of the flywheel

Eq . (47) shows the linear relation between the equivalent mass and the moment of inertia of the flywheel, $I_f$, . Figure 6-15 shows the linear relation between the both. Increasing the flywheel mass will result into a larger equivalent mass and thus, the energy output is significantly affected which is seen in Figure 6-16

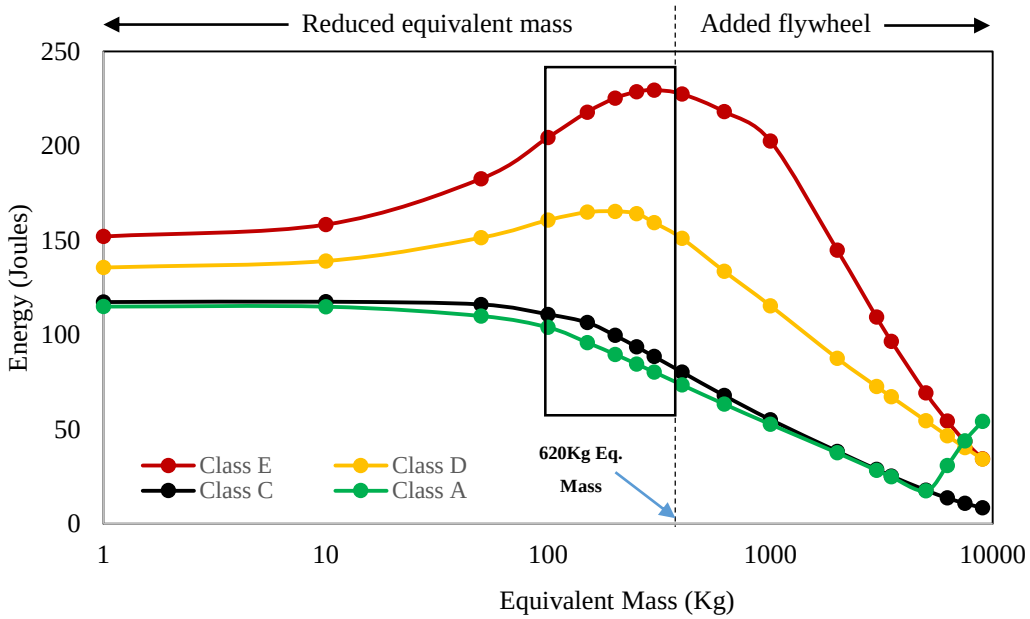


Figure 6-16 Effects of flywheel mass onto the power generation- total energy

As we see in the figure, adding a flywheel doesn't really helps getting more energy output, instead, if the overall equivalent mass is decreased, the overall energy output increases. The rectangular box in the Figure 6-16 represents range or region in which equivalent mass will yield maximum overall energy output for all classes of vehicles.

## 6.6 Lab and in-field test results

As discussed earlier in section 5, the experiments are divided into two parts. Lab and the in-field test. Since, the prototype is really big, it was virtually impossible to carry all pre-examinations of the prototype outside of the lab environment. To measure the effectiveness of the system, three people are made to jump on the cover in order to generate power in the harvester. The output voltage in Figure 6-17 (a), verifies the effectiveness of mechanical motion rectifier mechanism. The measure acceleration and displacement in Figure 6-17 (b) right, demonstrate that the vertical vibration is much large than that in horizontal direction.

Despite the harvester is driven by weights of three persons with much lower force and smaller amplitude, less than 10% of a passage car, the output voltage is still large enough with peak voltage up to 60W as shown in Figure 6-18 (b), which lights up three 60W bulbs shown in

previous section 5 in Figure 5-1. This regenerated energy power is much larger than the harvesting capacity in almost all the current literatures reviewed in chapter 2. The resistor of 60W and 110V lights is 201 Ohm. The current between two phases is measured using a 1 Ohm resistor as shown in Figure 6-17 (a), and the external resistor of 202 Ohm, which is corresponding to the equivalent damping of 213 N.s/m.

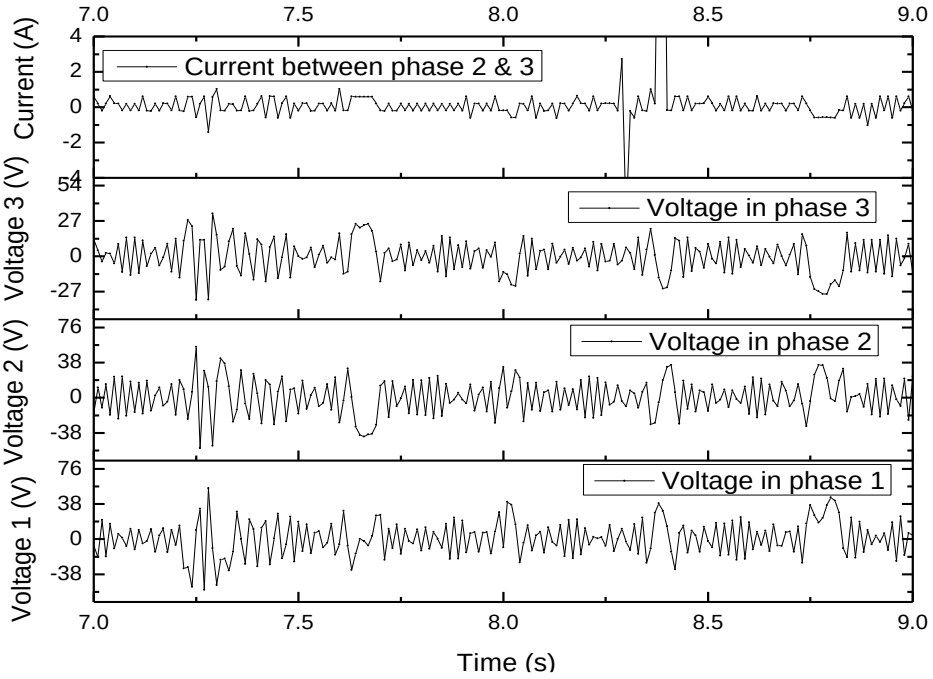


(a)

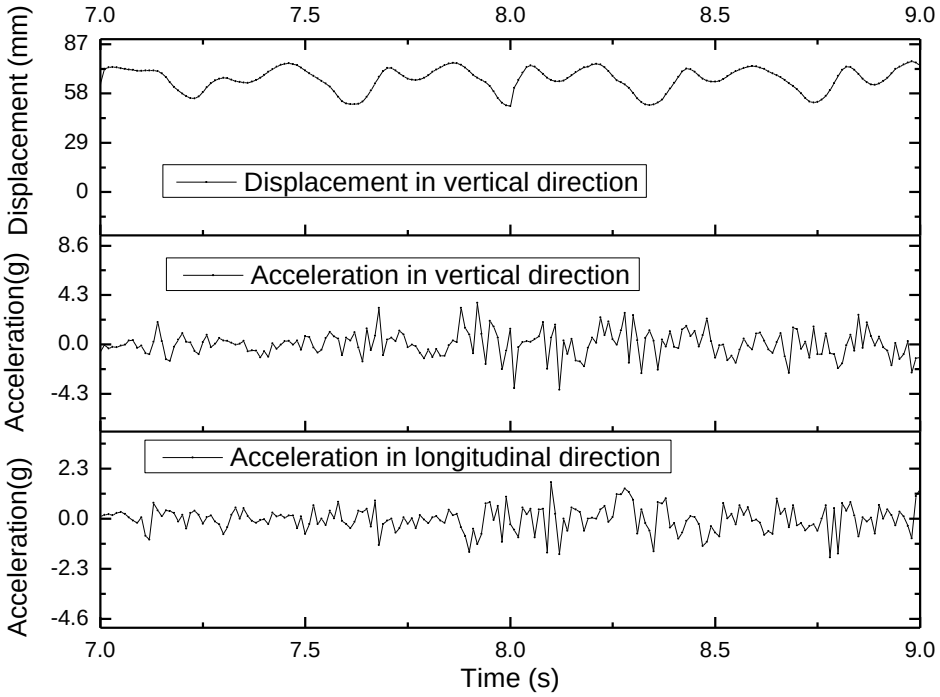


(b)

Figure 6-17 (a) Voltage and current in the external resistant of generator and Dynamic performance. (b) Displacement and accelerations of the sprung mass

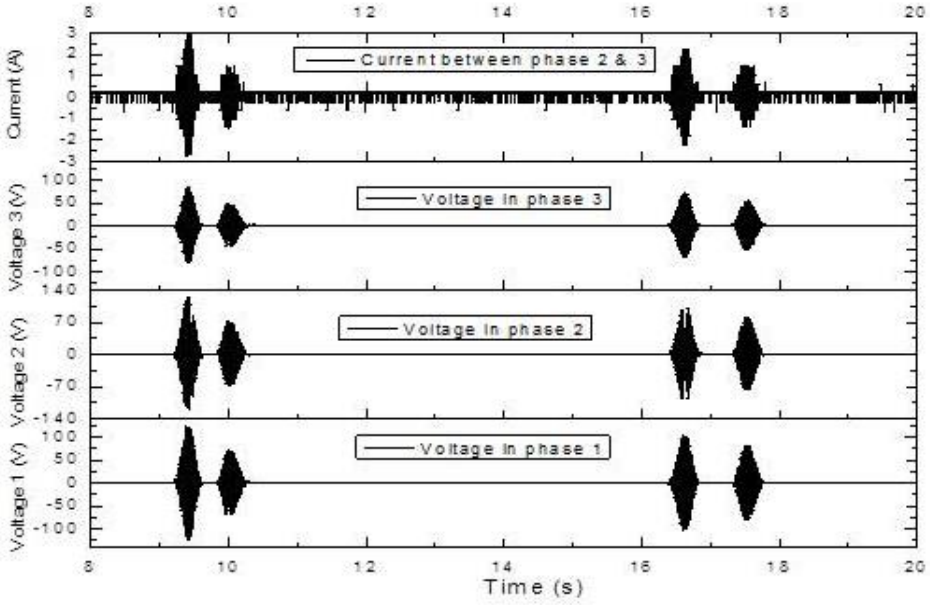


(a)

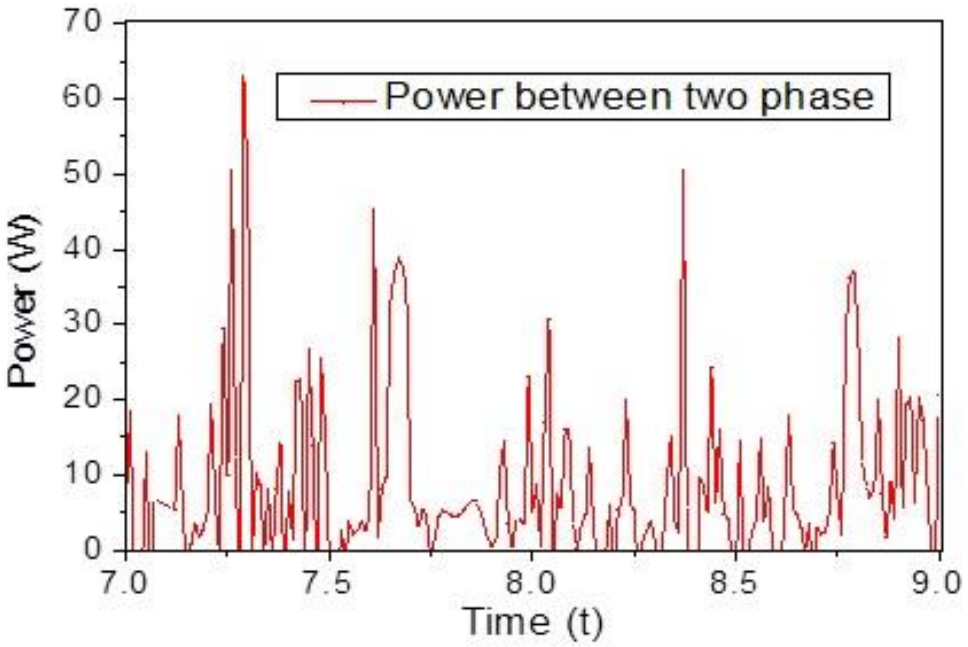


(b)

Figure 6-18 (a) generated current and voltage between three phases of BDCL motor. (b) Power generated between two phases

On the other hand, in-field test is carried out by mocking up the real scenarios of harvester inserted between two wood trails to permit vehicle driving along and passing over the speed bump energy harvester, as shown in previous section 5 in figure 5-4. A convenient test platform is developed with speed bump for vehicle to pass through the speed bump as does on road. The experimental results about the speed bump displacement and power are shown in Figure 6-19 and Figure 6-20 respectively, in which the vehicle was driven in front and back directions so that the front axles passed the speed bump energy harvester twice in opposite directions.

When the test car passes over the speed bump energy harvester, the measured displacement of speed bump energy harvester is shown in Figure 6-19. The speed bump cover goes down quickly reach to the bottom limiter from 3.138s and 3.374s and from 9.198s and 9.404s. The ac generator of the MMR-based speed bump energy harvester rotates to produce electrical voltage when the speed bump cover was pressed to move downward, as illustrated in figure 6-20 (a). The regenerated voltage is shown in Equation (5). The calculated peak power from two terminals of

the three-phase generator, as shown in figure 6-20 (b), can reach up to 541w and 646.6w with the maximum voltage of 118v and 120v respectively. The total peak power of the whole generator will be $\sqrt{3}$ x541~647w =937~1120w.

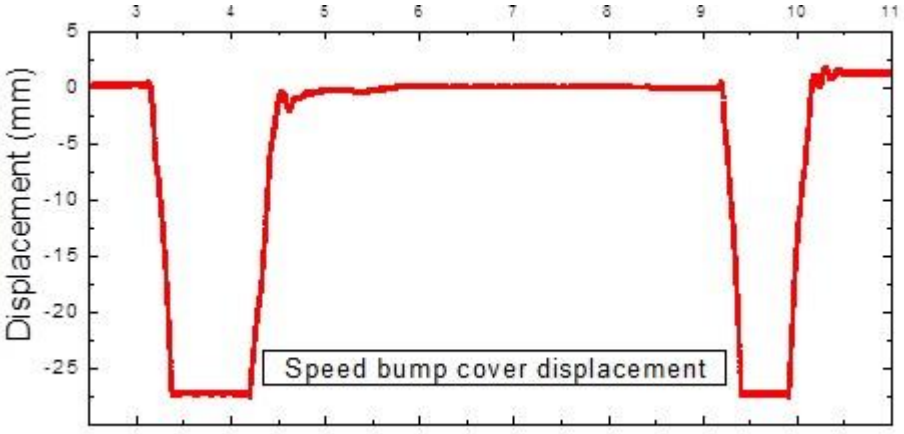


Figure 6-19 Displacement of the speed bump cover as measured by the laser displacement sensor

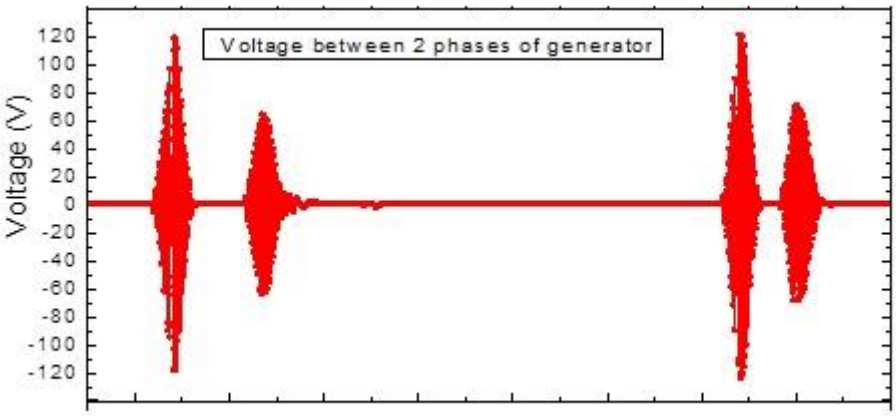


(a)

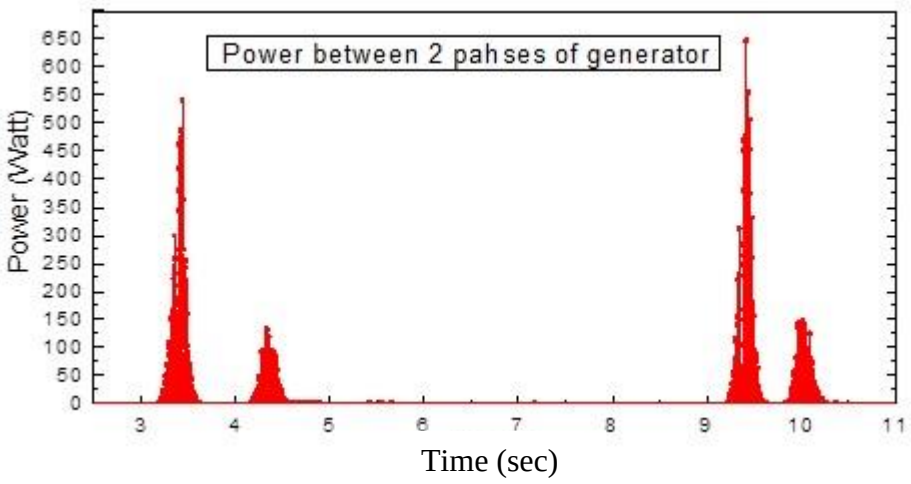


(b)

Figure 6-20 Total power generated between two phases of BLDC generator during the in-field test (a) generated voltage (b) generated power

After the speed bump cover reaches its bottom limitation, it can't move anymore as shown in Figure 6-19; however, the generator shaft can still rotate freely with disengagement of one-way clutch and continue producing electricity from the rotating inertia till the rotation stops, as shown in Figure 6-20(b), which keeps generating the power until the rotation speed of the shaft dies out. We can see that such working mechanism of MMR has the advantage in converting and storage of the large-scale impulse vibration energy in short time and continuously producing electricity in longer duration by continuous rotation of generator using disengagement of MMR, even though the movement of the speed bump cover stopped.

After the vehicle tires pass the speed bump cover, the speed bump energy harvester cover was rebounded upward by the forces from the four supporting springs from 3.42s and 3.672s and from 9.414s and 9.642s. When the cover moves upward, the one-way clutch in MMR is engaged and drives the generator to produce electricity in the same direction as driven downward. When the cover stops movement, the generator continuously rotates to produce more energy. As shown in Figure 6 -20 (b) the harvested power from the rebounding motions can reach the peak power of 131W with voltage of 65V and 145W with the voltage peak of 68V respectively. We can also see that the MMR has the advantages in producing electrical power by transferring both down and up movement into unidirectional movement and regenerating more electricity. The recovered energy

during this rebounding process is almost at the same level of 70V, which is determined by the harvester parameters including the supported horizontal speed. Only the vertical dynamic performance of speed bump energy harvester and vehicle is considered (according to the experimental results in Figure 6-21 the vertical vibration is much larger than horizontal vibration). The horizontal displacement of vehicle is calculated by $x = V \cdot t$, where $V$ is the vehicle speed and $t$ is the time after tires touch the speed bump cover.

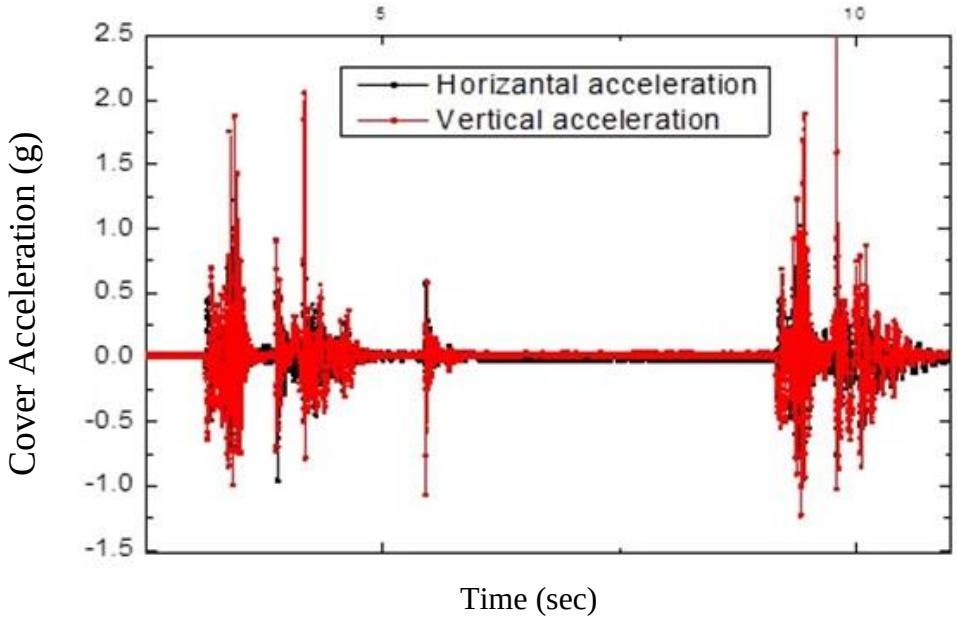


Figure 6-21 Speed bump cover acceleration

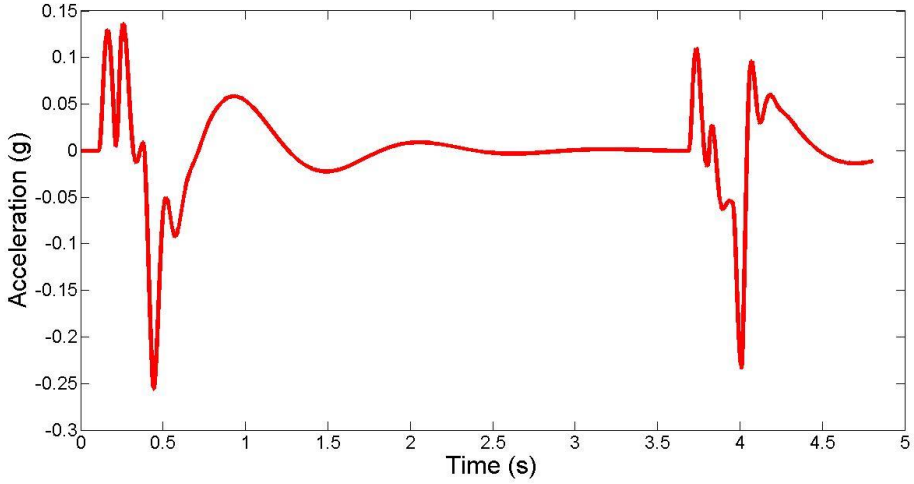

(a)

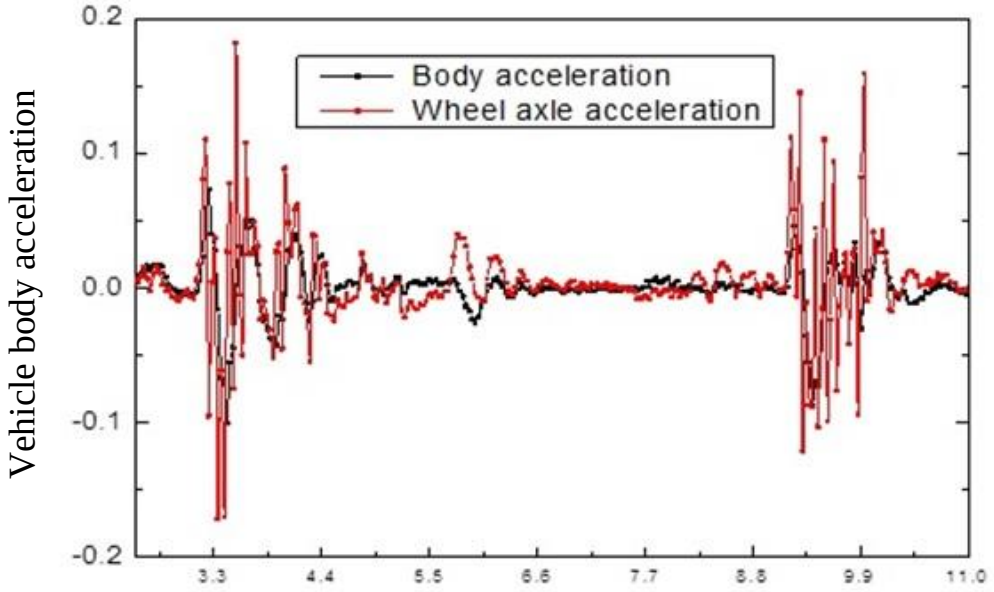


(b)

Figure 6-22 accelerations of the vehicle sprung mass at 2 MPH(a) simulated result (b) in-field test result

In figure 6-22, the range of vehicle sprung mass acceleration as calculated in the simulation is strikingly close to the in-field test. This verifies the theoretical modelling and the approach towards measuring the vehicle dynamics responses.

# 7 Conclusion and future work

In this work, a new speed bump energy harvester has been investigated and developed with the scientific methodology and procedure. A thorough study of the speed bump and its geometry is conducted and a way to harvest large scape electrical power is proposed. Since, vehicle dynamics plays an important role in the development of such as energy harvester, the implications of such a harvester on the dynamics of the vehicle is also studied in depth. The capacity of the speed bump energy harvester to generate electricity is validated both by simulation and experimental data which includes a lab test and an in-field test. MATLAB model has been built to investigate the simulation results and is validated by the experimental data. In conclusion, it can be said that, the speed bump energy harvester prototype which is built has a capacity to generate about 600 watts of peak electrical power and about 200 watts of RMS power which can be further extended up to 1 kilo-watts of power.

The effectiveness of the mechanical motion rectifier design is concluded by comparing areas under the curve of power generated by MMR based harvester and the traditional electromagnetic harvester which suggests that MMR based harvester generates about 4-5 times more energy, which demonstrates it advantages over traditional one for energy harvesting from the pulse-like excitations. The presented novel speed bump energy harvester and its compact structure can conveniently replace the existing traditional speed bumps with less impact to the dynamics of the passing vehicles. The proposed speed bump energy harvester.is expected to provide sufficient electricity for many road side devices like signs, monitoring sensor and so on, which provide a cost-efficient energy source to supply electricity to intelligent transportation system especially in the areas where power grid cannot be accessed economically.

This can be said that, the present prototype is the forerunning design of the future concepts of similar speed bump harvester. This research opens a new area of research and invites the researchers and engineers to work on it. There are several improvement opportunities that one should think of. By investigating into following areas, the future scholar can extend the work to a un-precedence level:

1. Various parts have not been optimized in the research such as speed bump cover profile It will certainly be an interesting area to explore and to optimize the various component's parameters to harness maximum power out of the harvester.
2. Since there are various small and big components involved in the development of the harvester, and there is a large force and stresses involved in the individual components, it will be interesting to perform stress analysis on critical components such as, connecting rod, speed bump cover, base plate, and rack and pinion gear assembly. Their failure modes can be looked into and the future scholar can work on improving the overall efficiently of the device.
3. More in-depth analysis of the vehicle dynamics should be looked into. Tire dynamics, which is not mainly focused here, can also be an interesting area of research.
4. Last but not the least, the more comprehensive and rigorous in-field testing is required to analyze the real impact of the vehicle onto the speed bump energy harvester.

# 8 References


[1] "Intelligent Traffic Signal System." [Online]. Available: http://www.iteris.com/cvria/html/applications/app43.html. [Accessed: 30-Mar-2016].

[2] "Networked Traffic Lights Could Save Time, Fuel, and Lives : TreeHugger." [Online]. Available: http://www.treehugger.com/cars/networked-traffic-lights-could-save-time-fuel-and-lives.html. [Accessed: 30-Mar-2016].

[3] "Could smart traffic lights stop motorists fuming? | New Scientist." [Online]. Available: https://www.newscientist.com/article/dn13306-could-smart-traffic-lights-stop-motorists-fuming/. [Accessed: 30-Mar-2016].

[4] S. Fuchs, S. Rass, B. Lamprecht, and K. Kyamakya, "Context-Awareness and Collaborative Driving for Intelligent Vehicles and Smart Roads," *1st Int. Work. ITS an Ubiquitous ROADS 1st Glob. Inf. Infrastruct. Symp. (GIIS 07)*, pp. 1–6, 2007.

[5] P. Varaiya, "Smart cars on smart roads. Problems of control," *IEEE Trans. Automat. Contr.*, vol. 38, no. 2, pp. 195–207, 1993.

[6] S. S. Chavan, R. S. Deshpande, and J. G. Rana, "Design of Intelligent Traffic Light Controller Using Embedded System," *2009 Second Int. Conf. Emerg. Trends Eng. Technol.*, pp. 1086–1091, 2009.

[7] M. S. Shehata, J. Cai, W. M. Badawy, T. W. Burr, M. S. Pervez, R. J. Johannesson, and A. Radmanesh, "Video-based automatic incident detection for smart roads: The outdoor environmental challenges regarding false alarms," *IEEE Trans. Intell. Transp. Syst.*, vol. 9, no. 2, pp. 349–360, 2008.

[8] J. Malik, J. Weber, Q. T. Luong, and D. Koller, "Smart cars and smart roads," *Br. Mach. Vis. Conf. Birmingham, UK*, pp. 367–382, 1995.

[9] M. Jokela, M. Kutila, J. Laitinen, F. Ahlers, N. Hautière, and A. I. Road, "Optical Road Monitoring of the Future Smart Roads – Preliminary Results," *Int. J. Comput. Inf. Eng.*, vol. 23, no. August, pp. 502–507, 2007.

[10] M. Karpiriski, A. Senart, and V. Cahill, "Sensor networks for smart roads," *Fourth Annu. IEEE Int. Conf. Pervasive Comput. Commun. Work.*, p. 5 pp. –310, 2006.

[11] U.S. Energy Information Agency, "International Energy Outlook 2013," *Outlook 2013*, p. 312, 2013.

[12] I. P. O. C. C. IPCC, "IPCC Special Report on Renewable Energy Sources and Climate Change Mitigation Summary for Policymakers," no. May 2011, pp. 5–8.

[13] C. Change, T. Greater, M. Subregion, and M. Information, "Bio-Brief # 2 : Climate Change  Changing Climate & the," pp. 2009–2010, 2013.

[14] S. Bachu, "Screening and ranking of sedimentary basins for sequestration of CO2 in geological media in response to climate change," *Environ. Geol.*, vol. 44, no. 3, pp. 277–289, 2003.

[15] N. (IIASA) Nakicenovic, "Global Energy Perspectives: Efficiency and Decarbonization Revolution," *ALPS Int. Symp.*, 2012.

[16] "EIA - Electricity Data." [Online]. Available: http://www.eia.gov/electricity/monthly/epm_table_grapher.cfm?t=epmt_1_01. [Accessed: 15-Mar-2016].

[17] "Electricity in the United States - Energy Explained, Your Guide To Understanding Energy

- Energy Information Administration." [Online]. Available: http://www.eia.gov/energyexplained/index.cfm?page=electricity_in_the_united_states. [Accessed: 12-Mar-2016].
[18] Directorate of Global Energy Economics, "India Energy Outlook," 2015.
[19] I. Allocated, S. In, and C. S. Utilities, "Northern Region Western Region," 2014.
[20] C. A. Committee, "Coal in the Energy Supply of China," *IEA Coal Ind. Advis. Board*, pp. 1–110, 2000.
[21] M. Hoel Snorre Kvemdokk, "Depletion of fossil fuels and the impacts of global warming," *Resour. Energy Econ.*, vol. 18, no. 0928, pp. 115–136, 1996.
[22] S. Shafiee and E. Topal, "When will fossil fuel reserves be diminished?," *Energy Policy*, vol. 37, no. 1, pp. 181–189, 2009.
[23] T. K. Mideksa and S. Kallbekken, "The impact of climate change on the electricity market: A review," *Energy Policy*, vol. 38, no. 7, pp. 3579–3585, 2010.
[24] "US Vehicle Registration Data Statistics | Fast Delivery | United States Car, Motorcycle and Light Truck Stats - Hedges & Company." [Online]. Available: https://hedgescompany.com/automotive-market-research-statistics/auto-mailing-lists-and-marketing#facts. [Accessed: 12-Mar-2016].
[25] R. B. Goldner, P. Zerigian, and J. R. Hull, "A Preliminary Study of Energy Recovery in Vehicles by Using Regenerative Magnetic Shock Absorbers," *Sae Tech. Pap. Ser.*, no. 724, 2001.
[26] Z. Li, L. Zuo, J. Kuang, and G. Luhrs, "Energy-harvesting shock absorber with a mechanical motion rectifier," *Smart Mater. Struct.*, vol. 22, no. 2, p. 025008, Feb. 2013.
[27] Z. Li, L. Zuo, G. Luhrs, L. Lin, and Y. Qin, "Electromagnetic Energy-Harvesting Shock Absorbers: Design, Modeling, and Road Tests," *IEEE Trans. Veh. Technol.*, vol. 62, no. 3, pp. 1065–1074, Mar. 2013.
[28] X. Tang and L. Zuo, "Enhanced vibration energy harvesting using dual-mass systems," *J. Sound Vib.*, vol. 330, no. 21, pp. 5199–5209, Oct. 2011.
[29] X. Tang and L. Zuo, "Vibration energy harvesting from random force and motion excitations," *Smart Mater. Struct.*, vol. 21, no. 7, p. 075025, Jul. 2012.
[30] J. Wang, T. Lin, and L. Zuo, "DETC2013-12770 High Efficiency Electromagnetic Energy Harvester for Railroad Application," pp. 1–10, 2013.
[31] L. Zuo and P.-S. Zhang, "Energy Harvesting, Ride Comfort, and Road Handling of Regenerative Vehicle Suspensions," *J. Vib. Acoust.*, vol. 135, no. 1, p. 011002, Feb. 2013.
[32] M. Pau and S. Angius, "Do speed bumps really decrease traffic speed? An Italian experience.," *Accid. Anal. Prev.*, vol. 33, no. 5, pp. 585–97, Sep. 2001.
[33] M. Parkhill, P. Eng, R. Sooklall, M. a Sc, and G. Bahar, "Updated Guidelines for the Design and Application of Speed Humps," *Annu. Meet. Exhib. Compend. Tech. Pap.*, p. 13, 2007.
[34] "'Democratic Rate Plan Favored by Roosevelt [and other news]'. New York Times. 1906-03-07. p. 3." [Online]. Available: http://query.nytimes.com/mem/archive-free/pdf?res=9403E0DA1531E733A25754C0A9659C946797D6CF. [Accessed: 12-Mar-2016].
[35] "Who invented Speed bumps?; Arthur Holly Compton in; Reason; Variations; Fans of the Speed Bump." [Online]. Available: http://layerdrain.com/article/who-invented-speed-bumps. [Accessed: 12-Mar-2016].
[36] "What is Traffic Calming? | Traffic Calming Solutions | TrafficLogix." [Online]. Available: http://trafficlogix.com/trafficcalming/trafficcalming. [Accessed: 14-Mar-2016].

[37] L. Johnson and a J. Nedzesky, “A Comparative Study of Speed Humps , Speed Slots and Speed Cushions,” *ITE Annu. Meet. Exhib.*, p. 14, 2004.
[38] S. Arabia, “DYNAMIC CONSIDERATIONS OF SPEED CONTROL HUMPS ( a ) Hump profile,” vol. I, no. 4, pp. 291–302, 1982.
[39] D. Garcia-Pozuelo, A. Gauchia, E. Olmeda, and V. Diaz, “Bump Modeling and Vehicle Vertical Dynamics Prediction,” *Adv. Mech. Eng.*, vol. 2014, pp. 1–10, 2014.
[40] J. P. Hessling, “Road Humps,” pp. 1–23, 2008.
[41] E. Khorshid, F. Alkalby, and H. Kamal, “Measurement of whole-body vibration exposure from speed control humps,” *J. Sound Vib.*, vol. 304, no. 3–5, pp. 640–659, Jul. 2007.
[42] A. Mitra, N. Benerjee, H. A. Khalane, M. A. Sonawane, D. R. Joshi, and G. R. Bagul, “Simulation and Analysis of Full Car Model for various Road profile on a analytically validated MATLAB / SIMULINK model,” pp. 22–33, 1997.
[43] T. A. O. Salau, S. A. Oke, and A. O. Adeyefa, “Vehicle Speed Control Using Road Bumps : Part 2,” *Transport*, vol. XX, no. 3, pp. 99–105, 2005.
[44] G. Watts, *Road humps for the control of vehicles speeds*. Crowthorne: Road User Characteristics Div. Safety Dep. Transport and Road Research Laboratory, 1973.
[45] H. Ansari Ardeh, M. Shariatpanahi, and M. Nikkhah Bahrami, “Multiobjective shape optimization of speed humps,” *Struct. Multidiscip. Optim.*, vol. 37, no. 2, pp. 203–214, Feb. 2008.
[46] D. Pešic, M. Vujanic, and K. Lipovac, “Safety Scien ce The influence of speed bumps heights to the decrease of the vehicle speed – Belgrade experience,” vol. 57, pp. 303–312, 2013.
[47] S. Aslan, O. Karcioglu, Y. Katirci, H. Kandiş, N. Ezirmik, and O. Bilir, “Speed bump-induced spinal column injury,” *Am. J. Emerg. Med.*, vol. 23, no. 4, pp. 563–564, 2005.
[48] C. C. Smith, D. Y. McGehee, and a. J. Healey, “The Prediction of Passenger Riding Comfort From Acceleration Data,” *J. Dyn. Syst. Meas. Control*, vol. 100, no. 1, p. 34, 1978.
[49] J. Granlund and A. Brandt, “Bus Drivers ’ Exposure To Mechanical Shocks Due To Speed Bumps,” no. 8, pp. 1–10.
[50] P. Taylor, T. Abiola, O. Salau, A. O. Adeyefa, and S. A. Oke, “Vehicle speed control using road bumps,” no. December 2014, pp. 37–41.
[51] C. Johansson, P. Rosander, and L. Leden, “Distance between speed humps and pedestrian crossings: Does it matter?,” *Accid. Anal. Prev.*, vol. 43, no. 5, pp. 1846–1851, 2011.
[52] M. Azman, P. D. King, and H. Rahnejat, “Combined bounce, pitch, and roll dynamics of vehicles negotiating single speed bump events,” *Proc. Inst. Mech. Eng. Part K J. Multi-body Dyn.*, vol. 221, pp. 33–40, 2007.
[53] J. P. Hessling, “Analysis of Vehicle Rotation during Passage over Speed Control Road Humps,” pp. 304–308, 2008.
[54] E. H. Technologies, *Priya, Shashank, and Daniel J. Inman, eds. Energy harvesting technologies. Vol. 21. New York: Springer, 2009.* .
[55] “Piezoelectric Roads in California.” [Online]. Available: http://large.stanford.edu/courses/2012/ph240/garland1/. [Accessed: 09-Feb-2015].
[56] D. Chambers, “FINAL PROJECT REPORT ASSESSMENT OF PIEZOELECTRIC MATERIALS FOR ROADWAY ENERGY Cost of Energy and Demonstration Roadmap,” 2014.
[57] S. Andriopoulou, “A review on energy harvesting from roads.,” pp. 1–39, 2012.
[58] C. K. Das, S. M. Hossain, and M. S. Hossan, “Unit for Minor Needs,” 2013.

[59] B. S. Sarma, V. Jyothi, and D. Sudhir, “Design of Power Generation Unit Using Roller Mechanism,” *Iosr - Jeee*, vol. 9, no. 3, pp. 55–60, 2014.
[60] A. Tank and K. Shah, “Eco-Friendly Energy Generation through Speed Breaker,” vol. 2, no. 1, pp. 1232–1235, 2014.
[61] “Speed Bumps Harvest Electricity from Moving Cars | Inhabitat - Green Design, Innovation, Architecture, Green Building.” [Online]. Available: http://inhabitat.com/speed-bumps-harvest-electricity-from-moving-cars/. [Accessed: 12-Mar-2016].
[62] “Speed-bump device converts traffic energy to electricity.” [Online]. Available: http://phys.org/news/2011-11-speed-bump-device-traffic-energy-electricity.html. [Accessed: 12-Mar-2016].
[63] A. Pirisi, F. Grimaccia, M. Mussetta, and R. E. Zich, “Novel speed bumps design and optimization for vehicles’ energy recovery in smart cities,” *Energies*, vol. 5, no. 11, pp. 4624–4642, 2012.
[64] A. Pirisi, M. Mussetta, F. Grimaccia, and R. E. Zich, “Novel speed-bump design and optimization for energy harvesting from traffic,” *IEEE Trans. Intell. Transp. Syst.*, vol. 14, no. 4, pp. 1983–1991, 2013.
[65] S. A. Ahmad, “Power Scavenging from Moving Vehicles on Road,” 2010.
[66] Z. Zhang, X. Zhang, Y. Rasim, C. Wang, B. Du, and Y. Yuan, “Design, modelling and practical tests on a high-voltage kinetic energy harvesting (EH) system for a renewable road tunnel based on linear alternators,” *Appl. Energy*, vol. 164, no. October 2015, pp. 152–161, 2016.
[67] “Institute of Transportation Engineers (ITE).” [Online]. Available: http://www.ite.org/traffic/hump.asp. [Accessed: 12-Mar-2016].
[68] Z. Li, L. Zuo, J. Kuang, and G. Luhrs, “Energy-harvesting shock absorber with a mechanical motion rectifier,” *Smart Mater. Struct.*, vol. 22, no. 2, p. 025008, 2013.
[69] P. Density, H. Reliable, and R. Compliant, “BLY34 Series - Brushless DC Motors •,” no. 714.
[70] T. Zumin, “United States Patent [ 19 ],” pp. 1–5, 1980.
[71] R. Vignaud, “` United States Patent C ) ice,” pp. 3–7, 1970.
[72] A. . Fallis, “No Title No Title,” *J. Chem. Inf. Model.*, vol. 53, no. 9, pp. 1689–1699, 2013.
[73] P. For, T. H. K. Production, T. Sakakibara, K. Kaneko, and O. P. Docum, “United StateS Patent [19],” *Production*, pp. 2–6, 1982.
[74] P. Number, “United States Patent [19] [54],” pp. 0–4, 1984.
[75] “Planetary Gear Sets - Operation and Theory - Planetary Gearset Control Devices (continued).” [Online]. Available: https://wikis.engrade.com/planetarygearsetsoperati/planetarycontrols2. [Accessed: 12-Mar-2016].
[76] “Steel One-Way Locking Needle-Roller Bearing with Plastic Cage,” p. 6392, 2010.
[77] R. N. Jazar, *Vehicle Dynamics: Theory and Applications*. 2008.
[78] P. Todaria, L. Wang, A. Pandey, J. O’Connor, D. McAvoy, T. Harrigan, B. Chernow, and L. Zuo, “Design, modeling and test of a novel speed bump energy harvester,” vol. 9435, p. 943506, 2015.
[79] “MaineDOT Maine Local Roads Center: Speed Humps vs. Speed Bumps.” [Online]. Available: http://www.maine.gov/mdot/csd/mlrc/technical/shsb.htm. [Accessed: 15-Mar-2016].